Tectonics

RESEARCH ARTICLE
10.1029/2020TC006684

Key Points:

- 20°–30°CW post-Late Miocene rotation of the Cordillera Occidental, no rotation of the Cordillera Real, southern Ecuador
- The southern Cordillera Occidental emplaced as a rotational nappe after the late Miocene-Pliocene over the flexural Interandean Valley basin
- No paleomagnetic evidence for latitudinal terrane drift and orogen-parallel strike-slip activity since Mid-Late Eocene (~40 Ma)

Supporting Information:

Supporting Information may be found in the online version of this article.

Correspondence to:

G. Siravo,
gaia.siravo@ingv.it

Citation:

Siravo, G., Speranza, F., Mulas, M., & Costanzo-Alvarez, V. (2021). Significance of Northern Andes terrane extrusion and genesis of the Interandean Valley: Paleomagnetic evidence from the "Ecuadorian Orocline". *Tectonics*, *40*, e2020TC006684. https://doi.org/10.1029/2020TC006684

Received 24 DEC 2020
Accepted 21 JUN 2021

Significance of Northern Andes Terrane Extrusion and Genesis of the Interandean Valley: Paleomagnetic Evidence From the "Ecuadorian Orocline"

Gaia Siravo[1], Fabio Speranza[1], Maurizio Mulas[2], and Vincenzo Costanzo-Alvarez[3]

[1]Istituto Nazionale di Geofisica e Vulcanologia, Rome, Italy, [2]Escuela Superior Politécnica del Litoral, Facultad de Ingeniería en Ciencias de la Tierra, Guayaquil, Ecuador, [3]Department of Mechanical and Industrial Engineering, University of Toronto, Toronto, ON, Canada

Abstract GPS data suggest that the NW South America corner forms a semi-rigid block drifting NE-ward along the regional dextral strike-slip faults that bound an oceanic terrane accreted in Late Cretaceous times to W Ecuador and Colombia. However, the relevance of both strike-slip versus thrust tectonics during Cenozoic times and their relation with oceanic terrane accretion are unclear. Here we report on the paleomagnetism of 31 mid-upper Eocene to upper Miocene mainly volcanic sites from the Cordilleras Occidental and Real of southern Ecuador. Eleven sites show that the western Cordillera Occidental underwent a 24° ± 10° clockwise (CW) rotation with respect to South America after late Miocene times, while no rotation occurred further east. We relate the regional CW rotation to the emplacement of the Cordillera Occidental nappe onto the continental sediments of the Interandean Valley, blanketing the Cordillera's eastern margin. As rotation and continental sedimentation onset ages are similar, we interpret such tectonic depression as a narrow flexural basin formed ahead of the advancing nappe front. The 20°–30° CW Neogene rotation of the Cordillera Occidental is indistinguishable from the post-Cretaceous rotation of the Coastal forearc oceanic blocks, implying that the whole W Ecuador Andean chain was detached and rotated over a mid-crustal detachment during the last 10 Ma. Eocene-Miocene paleomagnetic inclination values are systematically consistent with those expected for South America, thus excluding latitudinal terrane drift. We suggest that the Andes of Ecuador and Peru form the "Ecuadorian Orocline", formed by opposing orogenic rotations around the Amazonian craton indenter.

1. Introduction

The northernmost Andes form an articulated orogenic system, arising from the interaction of the Panama Arc and the Nazca and Caribbean plates with the NW South America corner (e.g., Montes et al., 2012; Mora et al., 2017; Pennington, 1981; Trenkamp et al., 2002; Figure 1). Egbue and Kellogg (2010), Nocquet et al. (2014), Pennington (1981), and Trenkamp et al. (2002) considered the Northern Andes as a distinct tectonic block (Northern Andean Block).

GPS data (Alvarado et al., 2014; Nocquet et al., 2014; Pérez et al., 2018; Trenkamp et al., 2002; Villegas-Lanza et al., 2016; Figure 1) document a 0.6 cm/yr oblique NE-ward drift of the Northern Andes with respect to South America that is considered to be accommodated by orogen-parallel dextral strike-slip faults (Alvarado et al., 2016; Egbue & Kellogg, 2010; Jiménez et al., 2014; Nocquet et al., 2014; Pousse-Beltran et al., 2017; Trenkamp et al., 2002). This is consistent with an average 0.76 cm/yr Quaternary slip rate obtained from field investigation along the main strike-slip faults (Pallatanga and Cayambe-Afiladores faults; Egbue & Kellogg, 2010 and references therein). Nevertheless, pure thrust tectonics characterize the external (eastern) Northern Andes deformation front from Ecuador (e.g., Baby et al., 2013) to Colombia (e.g., Bayona et al., 2008).

Besides Quaternary-to-present kinematics, strike-slip tectonics is inferred to have occurred since the Late Cretaceous, along dextral faults that bounded oceanic-affinity terranes parallel to the Andean chain of Ecuador and Colombia (Alvarado et al., 2014; Daly, 1989; Egbue & Kellogg, 2010; Jiménez et al., 2014; Pousse-Beltran et al., 2017). The basement of the Ecuador Coastal forearc (Figure 1c) is made by upper Cretaceous, 88.8 ± 1.6 Ma (Ar^{39}/Ar^{40} dating by Luzieux et al., 2006), oceanic crustal terranes that were accreted to South America during a 70° clockwise (CW) rotation constrained at 70 Ma (Luzieux et al., 2006;

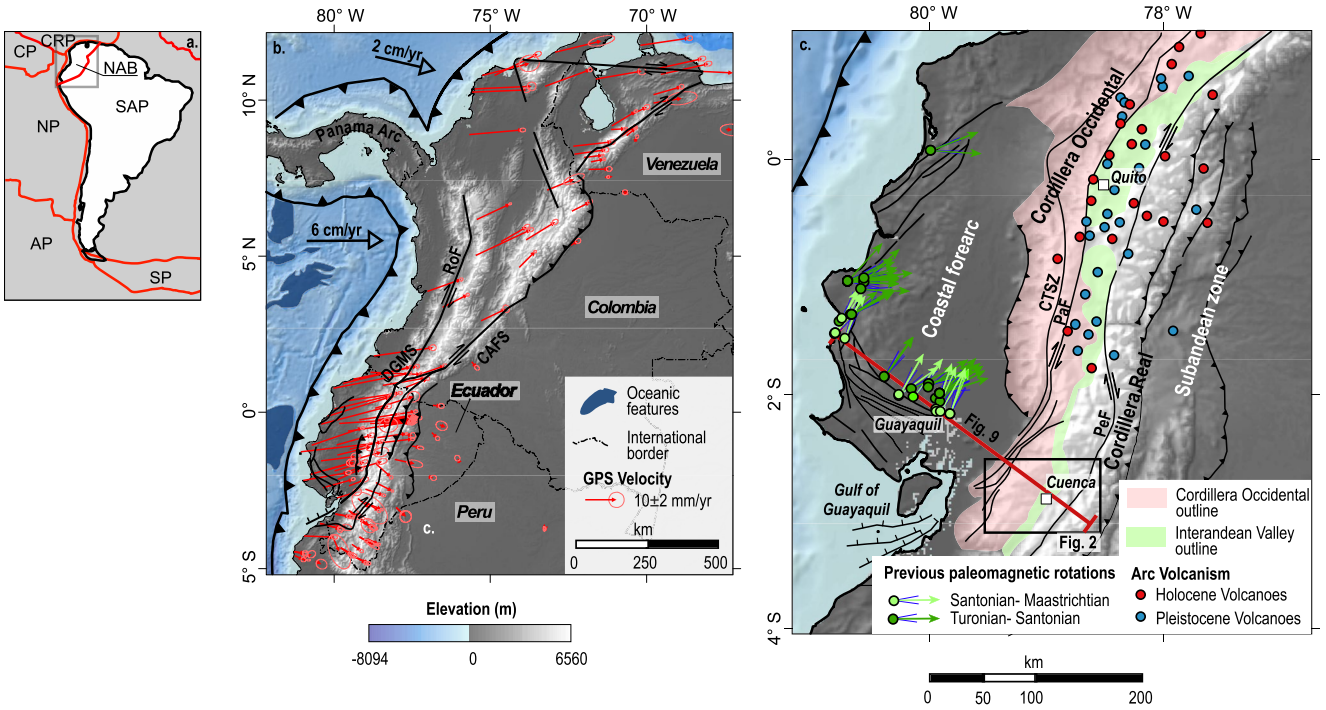

Figure 1. Tectonic setting of the northern Andes. (a) Schematic plate assemblage including the South American (SAP), Nazca (NP), and Caribbean plates (CRP), and the Northern Andean Block (NAB); the Antarctic (AP), Scotia (SP) and Cocos plates (CP) are shown for reference. (b) Main tectonic feature of the NW South America corner. GPS velocities of main plates (South America reference frame) are given with thick black arrows (Trenkamp et al., 2002), whereas GPS velocity and relative confidence limits from the NAB are shown with red arrows and ellipses (Trenkamp et al., 2002; Alvarado et al., 2014; Nocquet et al., 2014; Pérez et al., 2018). DGMS: Dolores-Guayaquil Mega Shear; RoF: Romeral Fault; CAFS: Cayambe-Afiladores Fault System. (c)) Tectonic features of the Ecuadorian Andes. Main strike-slip fault systems bound both the Cordilleras Occidental and Real; the Interandean valley is placed in between. Paleomagnetic rotations of data presented in Roperch et al. (1987) and Luzieux et al. (2006) recalculated with updated paleopoles of South America from Torsvik et al. (2012) are show as green arrows. Thick red line shows the location of the geologic section of Figure 9; black rectangle shows the location of Figure 2. CTSZ: Chimbo-Toachi Shear Zone; Paf: Pallatanga Fault; Pef: Peltectec Fault.

Roperch et al., 1987). The chemical composition and age similarity of oceanic crust from Ecuador (and Colombia) coastal terranes and cuttings from ODP wells drilled within the Caribbean plate led to the widely accepted suggestion that the W Ecuador-Colombia terranes are fragments of the Caribbean plate left behind during its drift from an original paleo-Pacific location (Kerr et al., 1997, 2002; Kerr & Tarney, 2005; Luzieux et al., 2006; Massonne & Toulkeridis, 2012; Spikings et al., 2001; Vallejo et al., 2009). Preliminary paleomagnetic data from the W Colombia Cordillera (Hincapié-Gómez et al., 2018; Montes et al., 2005), and the robust data set from Coastal Ecuador terranes (Luzieux et al., 2006; Roperch et al., 1987) were used to suggest a Caribbean origin at shallow southern Pacific latitudes and subsequent northward drift.

In this framework, the following issues are still unclear: (a) did the Northern Andean Block kept drifting northward during the Cenozoic? (b) Was such drift accommodated by individual faults or did it involve the northern Andes as a whole (e.g., Jiménez et al., 2014)? (c) How significant was strike-slip tectonics when compared to thrust tectonics during Cenozoic times?

The incertitude on the magnitude of a hypothetical Cenozoic strike-slip deformation is reflected by the variable interpretations of the tectonic regime that generated the Ecuadorian Interandean Valley (Figure 1). This tectonic depression, blanketing the eastern side of the Cordillera Occidental, has been variably considered as due to extensional, thrust, or strike-slip tectonics (Hungerbühler et al., 2002; Lavenu et al., 1995; Noblet & Marocco, 1989; Steinmann et al., 1999; Tibaldi & Ferrari, 1992; Villagómez, 2003; Winkler et al., 2005).

Paleomagnetism may represent an important tool to unravel the Cenozoic tectonic history of the Northern Andean Block, as peculiar patterns of vertical axis rotations arise from strike-slip (e.g., England & McKenzie, 1982; England & Wells, 1991; England et al., 1985; Nelson & Jones, 1987; Piper et al., 1997; Sonder &

England, 1986; Sonder et al., 1986, 1994) and thrust tectonics (e.g., Channell et al., 1990; Cifelli & Mattei, 2010; Maffione et al., 2009; Shaanan et al., 2015; Speranza et al., 2018; Weil et al., 2010).

Here we report on the first paleomagnetic data set from the Cordilleras Occidental and Real of Ecuador and attempt to untangle the relative contribution of thrust versus strike-slip tectonics in the development of the Ecuadorian Andes during mid-late Cenozoic times.

Our results indicate that no significant Cenozoic strike-slip deformation occurred in post-Eocene times and that the Cajas Plateau underwent a post-late Miocene 20°–30° CW rotation related to rotational thrust sheet emplacement west of the Azogues fault.

Finally, considering our results on a continental scale, in combination with previous paleomagnetic data from the Andean belt (Arriagada et al., 2008; Beck et al., 1994; Butler et al., 1995; Gilder et al., 2003; Lamb, 2001a, 2001b; Maffione et al., 2009; Narea et al., 2015; Prezzi et al., 2004; Riller & Oncken, 2003; Roperch & Carlier, 1992; Rousse et al., 2005), we suggest that the Andes of Ecuador and Peru form the "Ecuadorian Orocline" because of the opposite sign orogenic rotations around the Amazonian craton indenter.

2. Background

2.1. Geodynamic Context

The Ecuadorian Andes belong to the Northern Andean chain (Figure 1). Compared to the high plateaus of the Central Andes, they show lower mean elevation (~2,500), narrower width, and occurrence of exotic terranes interpreted as oceanic crust blocks accreted to South America during late Cretaceous times (Aspden & Litherland, 1992; Luzieux et al., 2006; Ramos, 2009; Spikings et al., 2005, 2010). The Northern Andes formed in a complex tectonic setting, characterized by the interaction of three main plates: South America, Nazca, and Caribbean (Figure 1a). GPS data show that—considering a South America fixed reference frame—the Nazca plate moves eastward by 6 cm/yr and subducts below the Andes, whereas the Caribbean plate drifts toward the ESE at ca. 2 cm/yr (Figure 1b).

Complex plate interaction gives rise to a wide deformation zone, extending from Ecuador to Colombia and Venezuela, characterized by both submarine/onshore accretionary wedges and seismically active dextral faults (Alvarado et al., 2016; DeMets et al., 2010; Mora et al., 2017; Pousse-Beltran et al., 2017; Trenkamp et al., 2002). After the study done by Pennington (1981), this Andean sector was considered as a proper microplate: the Northern Andean Block (NAB in Figure 1a), undergoing 0.6 cm/yr NNE-ward (Trenkamp et al., 2002) independent drift with respect to nearby plates (Cediel et al., 2003; Egbue & Kellogg, 2010; Ramos, 2009). The boundary between South America and NAB is assumed to coincide with both regional dextral strike-slip and reverse fault systems that extend from the Gulf of Guayaquil (Ecuador) to the gulf Triste (Venezuela), following main topographic ranges and changing strike and deformation style along their length (Figure 1; Baize et al., 2020; Egbue & Kellogg, 2010; Jiménez et al., 2014; Nocquet et al., 2014; Pousse-Beltran et al., 2017; Trenkamp et al., 2002). Active seismicity along both types of faults has been recorded and inferred for historical time (e.g., Beauval et al., 2010; Dimate et al., 2003; Paris, 2000). In addition, a compilation of dextral fault displacements from field constraints suggests variable slip rates from 0.4 to 1 cm/yr during the last 1.8 Ma (Baize et al., 2020; Egbue & Kellogg, 2010; Eguez et al., 2003; Pousse-Beltran et al., 2017). Dextral faults are assumed to have formed as Late Cretaceous suture zones, as oceanic terranes occur along the western NAB, and subsequently reactivated during Cenozoic times.

In Ecuador, the Dolores-Guayaquil megashear and the Peltectec faults are NE-trending dextral strike-slip fault systems that have been related to two distinct collisional events: the first spanning from Santonian-early Campanian (85–80 Ma) (Aspden et al., 1992; Kerr et al., 2002; Lebras et al., 1987; Spikings et al., 2005) to late Campanian-Maastrichtian (75–65 Ma) (Jaillard et al., 2004; Luzieux et al., 2006; Spikings et al., 2001, 2010), the second between Late Paleocene (Jaillard et al., 1995), or Eocene (Kerr & Tarney, 2005; Kerr et al., 2002) to Late Eocene-Oligocene (Spikings et al., 2005). Conversely, other works (e.g., Aizprua et al., 2019) suggested that a single west Ecuadorian Andes terrane existed prior to accretion to South America that broke up and rotated CW during and after collision (Luzieux et al., 2006; Vallejo et al., 2009, 2019; Spikings et al., 2010) and that the Nazca subduction trench was reestablished after the accretionary tectonic phase in the Early Eocene (Aizprua et al., 2019). Magnetostratigraphically-calibrated paleomagnetic data

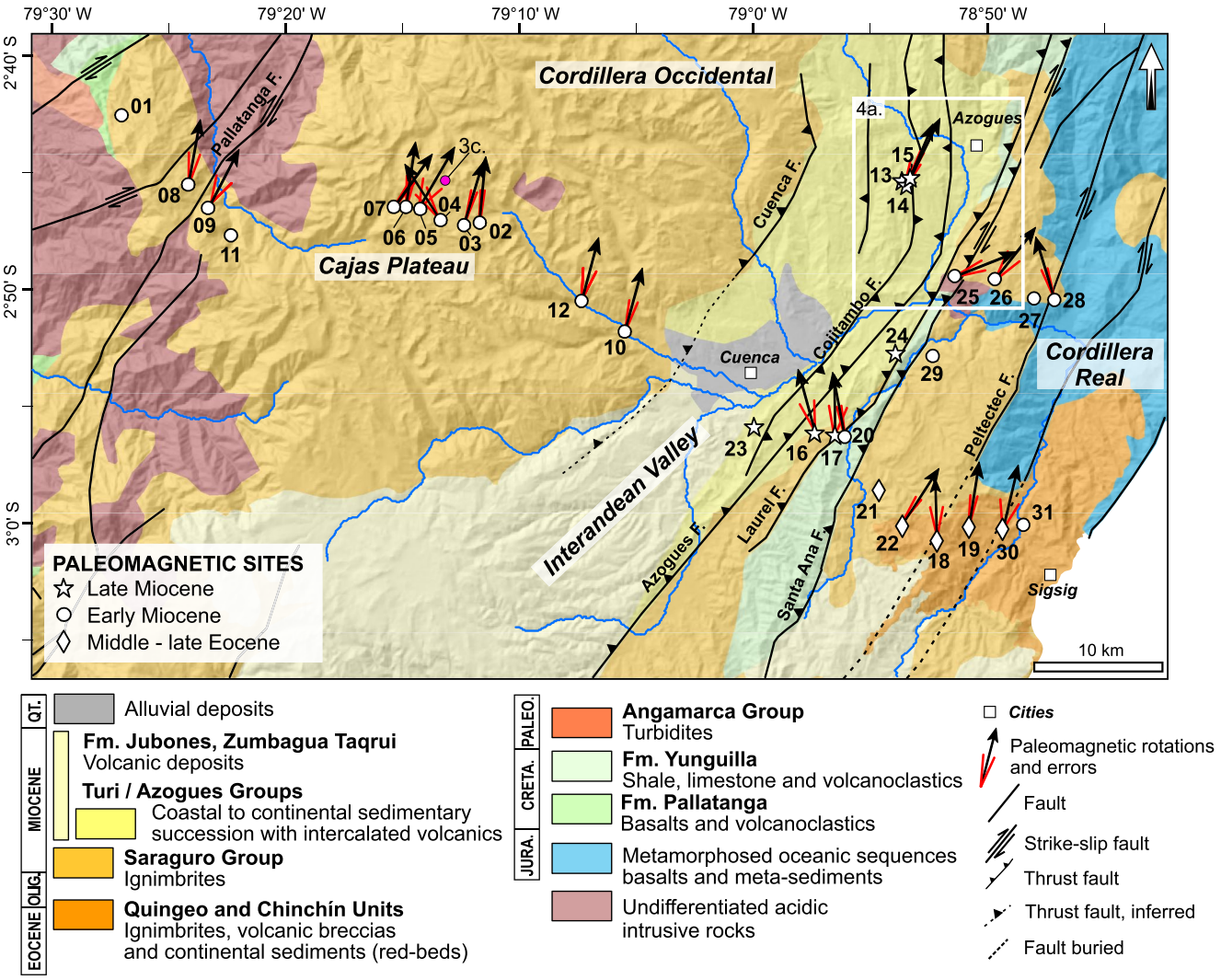

Figure 2. Geologic map of the southern Cordillera Occidental (Cajas Plateau), Interandean Valley, and Cordillera Real together with sampled paleomagnetic sites (symbols varying for sampled age) and vertical-axis rotations (black arrows; red angles indicate rotation error) calculated with respect to South America. White box is the location of the close-up map in Figure 4a.

from the W Ecuador oceanic terranes firmly show that a single episode of oceanic fragment accretion to South America was completed by early Maastrichtian times (ca. 70 Ma; Luzieux et al., 2006).

2.2. Regional Geological Setting and Features of the Study Area

From a tectonostratigraphic and geomorphologic point of view, the Ecuadorian Andes can be subdivided into five trench-parallel domains bounded by major faults (Figure 1). From West to East, the Coastal zone represents the fore-arc domain and is composed of upper Cretaceous mafic plume-related basement overlain by upper Cretaceous, and Paleocene to Miocene volcanoclastic sequences (e.g., Benitez, 1995; Gansser, 1973; Goossens & Rose, 1973; Jaillard et al., 1995, 1999). The Pallatanga fault marks the boundary between the Coastal fore-arc zone and the Cordillera Occidental, which consists of upper Cretaceous island arc volcanic rocks, oceanic-related fragments, plutons, and unconformable upper Cretaceous to Eocene turbidites. The Cordillera Occidental is intruded by middle Eocene to upper Cenozoic granites and is overlain by post-late Eocene continental arc volcanic rocks (Figure 2). North of 1.7°S, the Cordillera Occidental hosts active arc volcanism (Figure 1c; Global Volcanism Program, 2013).

The Pallatanga fault represents the southern segment of the regional Dolores - Guayaquil dextral megashear, which extends from the Gulf of Guayaquil to the Romeral fault in Colombia (Figure 1b). In detail, at its southernmost end, it displays a WSW–ENE trend and is characterized by an extensional horsetail structure that induced the opening of a pull-apart basin since 1.8 Ma (Witt & Bourgois, 2010; Witt et al., 2006). Northward, the Pallatanga fault system changes strike to SW-NE and SSW-NNE, cutting the western edge of the Cordillera Occidental with several splay faults from 3° to 2° 30′S. Further north, the N-S Chimbo-Toachi shear zone connects the Pallatanga and the Romeral fault in Colombia (Figure 1b). The main Pallatanga strand extends along the Cordillera Occidental and at ∼1°N joins to the East the Cayambe-Afiladores fault system in southern Colombia (Figure 1b). Relying on morphologic evidence, mean Holocene dextral slip rates of 3.5–4 mm/yr were reported along a Pallatanga fault splay from the central Ecuadorian Andes (Winter & Lavenu, 1989; Winter et al., 1993).

The contact between the Cordillera Occidental and the Cordillera Real is marked by the Peltectec fault. The roots of a Triassic–Jurassic volcanic arc emplaced into metamorphosed Paleozoic marine and volcanic sequence are exposed along the axis of the chain, whereas the western Cordillera Real comprises Triassic and Jurassic submarine basaltic–andesitic volcanic series (Aspden & Litherland, 1992; Litherland et al., 1994; Pratt et al., 2005). The Peltectec fault runs parallel to the Pallatanga fault with a NE trend south of 2°S. It gently bends to the NW at 2°S and continues to the NE from 1°S northward. At ∼1°N it connects with the Cayambe-Afiladores fault system and with the eastern Andes front in Colombia (Figure 1b). The fault has been considered as a late Jurassic (Aspden & Litherland, 1992; Litherland et al., 1994) or late Cretaceous (Spikings et al., 2001, 2005) shear zone that formed during the main deformation event of the Cordillera Real, after the accretion of the Cordillera Occidental block (Pratt et al., 2005). However, episodic exhumation events were inferred to cluster during the late Eocene, early Miocene, and Late Miocene to present (Spikings et al., 2001). Relying on thermochronologic data, the activity of the northern portion of the Peltectec fault has been inferred to span from 15 Ma to recent times (Spikings et al., 2010).

The Interandean Valley is a topographic depression straddling the two cordilleras, which comprises several distinct basins filled with volcano-sedimentary sequences deposited from the late Miocene onward (e.g., Winkler et al., 2005; Figure 1c). North of 2°S the Interandean Valley is bounded by the Pallatanga fault to the West and the Peltectec fault system to the East (Figure 1c). The activity of the Pallatanga fault was advocated as the cause for depression formation, although no agreement exists on the tectonics yielding depression onset. The Interandean Valley has been interpreted as (a) formerly extensional basin later reactivated by compressive tectonics (Villagómez, 2003), (b) transtensional (Tibaldi & Ferrari, 1992), (c) transpressive (Winkler et al., 2005), (d) strike-slip related (Noblet & Marocco, 1989), and (e) compressional basin (Hungerbühler et al., 2002; Lavenu et al., 1995; Steinmann et al., 1999). Moreover, the suggested age of tectonic activity comprises the entire Neogene (Hungerbühler et al., 2002; Lavenu et al., 1995; Noblet & Marocco, 1989; Steinmann et al., 1999; Tibaldi & Ferrari, 1992; Villagómez, 2003; Winkler et al., 2005).

South of 2°S the Interandean Valley lies some 50 km E of the Pallatanga fault and covers the eastern portion of the Cordillera Occidental. Here the deformation is dominated by closely spaced NE-trending thrust faults (Figure 2; Hungerbühler et al., 2002; Steinmann, 1997; Steinmann et al., 1999), and the Peltectec fault system and the Cordillera Real lie further East (Figure 2).

Our study focuses on the Cordillera Occidental, the Interandean Valley, and the Cordillera Real of Ecuador, between 2°40′ and 3°S (Figure 2). Here remnants of late Cretaceous oceanic terranes (Yunguilla and Pallatanga Formations in Figure 2) are overlain by Paleocene turbidites (Angamarca Group; e.g., Jaillard et al., 2004). Vigorous volcanic arc activity from the late Eocene (part of Quingeo and Chinchin units) to the early Miocene (Saraguro Fm.) yielded massive ignimbrite successions filling remnants of late Eocene and early Oligocene continental basins (part of Quingeo and Chinchin units (Hungerbühler et al., 2002; Steinmann, 1997; Figure 2). Particularly, the Saraguro Fm. largely outcrops in the area between the Pallatanga fault and the Cuenca city hereafter referred to as the Cajas Plateau. There, the welded early Miocene ignimbrite succession is generally sub-horizontal to gently tilted (Chiaradia et al., 2004; Mulas et al., 2017, Figure 3; Table 1).

Extensional tectonics occurring during the middle Miocene led to the formation of a coastal basin spanning the whole Ecuadorian Andes west of Cuenca (Steinmann, 1997; Hungerbühler et al., 2002). The

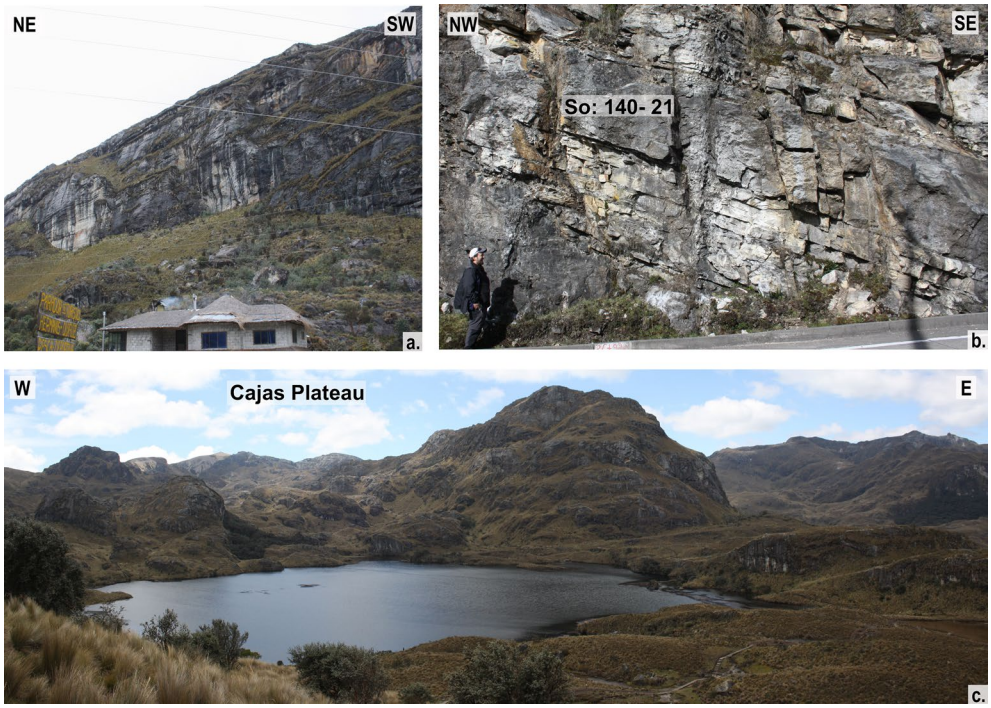

Figure 3. Field images from the Cajas Plateau (Saraguro Fm.) that display average low tilting ((a): site ECU07; (b) site ECU06) and no fault rupture. A general massive and undisturbed aspect is observed elsewhere (c).

sedimentary succession—preserved only in the Interandean Valley—consists of 2,700 m of fluvial, deltaic, brackish delta plain, lacustrine, and coastal sediments (Hungerbühler et al., 2002) firmly indicating that in mid-Miocene times the Cordillera Occidental was characterized by a coastal environment with marine influence (Bristow & Parodiz, 1982; Feldmann et al., 1993; Hungerbühler et al., 2002; Martínez-García et al., 2017; Nuttall, 1990; Steinmann, 1997). Steinmann et al. (1999) and Hungerbühler et al. (2002) proposed that during the mid-late Miocene this wide basin was inverted by E-W directed shortening, which also yielded the main exhumation event of the Cordillera Occidental.

During and after tectonic inversion, continental deposition took place only in the Interandean Valley that became the depocenter of sediments eroded from the Cordillera Occidental. A regional unconformity preserved in the Interandean Valley marks the transition from coastal deposits to continental sediments (Hungerbühler et al., 2002). The compressive deformation stage is well preserved in the Interandean depression by tilted and deformed Miocene coastal to continental strata (Figure 4). Thrust faulting and folding are observed along the valley (Figure 4b and 4c). West of the Cojitambo lava dome the increase of strata dip toward the East additionally suggests progressive tilting approaching a thrust-fault (Figures 3c and 4a). Steinmann et al. (1999) suggested that the Cojitambo lava dome (8 Ma) emplacement postdated the main deformation event and that late Miocene-Pliocene alluvial and pyroclastic air fall deposits seal the deformed basin fill.

To the East of the Interandean Valley, the Peltectec fault cuts Jurassic basalts and its trace fades out below Eocene to early Miocene volcanic (Figure 2). Finally, the Subandean zone to the East of the Cordillera Real is composed of steep east-verging thrust fronts forming the presently active Andean front (Legrand et al., 2005). Here compressive tectonics started in the Miocene and continued to present times (e.g., Baby et al., 2013; Roddaz et al., 2010).

3. Paleomagnetic Sampling and Methods

We aimed at paleomagnetically characterizing the Cordillera Occidental, the Interandean Valley, and the Cordillera Real, and constraining the rotations related to the main faults separating them. Consequently, samples were collected along an NW–SE transect, roughly from the Pallatanga to the Peltectec faults

Tectonics

10.1029/2020TC006684

Table 1
Paleomagnetic Directions From the Cordilleras Occidental and Real of Ecuador

Site	Lithology	Lat (°S)	Long (°W)	Unit in map 1:1.000.000 (1:50.000)	Age (Ma)	Bedding (dipdir -dip)	In-situ ChRM or HT						Tilt-corrected		Vertical-axis rotations				
							n/N	STATE	D (°)	I (°)	k (°)	α_{95} (°)	D (°)	I (°)	Pp (Ma)	R (°)	ΔR (°)	F (°)	ΔF (°)
ECU01[a]	Ignimbrite	2.710	79.450	Saraguro	Late Oligocene-Early Miocene (29.4 ± 2.6/19.0 ± 3.5)	144–36	9/10	-	-	-	-	-	-	-	-	-	-	-	-
ECU02	Ignimbrite	2.786	79.195	Saraguro	Late Oligocene-Early Miocene (29.4 ± 2.6/19.0 ± 3.5)	Sub-hzt	10/10	R	182.9	6.4	227.1	3.2	-	-	20	5.3	3.2	−8.2	4.6
ECU03	Ignimbrite	2.788	79.206	Saraguro	Late Oligocene-Early Miocene (29.4 ± 2.6/19.0 ± 3.5)	-	10/10	R	194.4	−4.9	194.4	3.5			20	16.6	3.4	−10.3	4.7
ECU04	Ignimbrite	2.784	79.223	Saraguro	Late Oligocene-Early Miocene (29.4 ± 2.6/19.0 ± 3.5)	Sub-hzt	9/10	R	145.0	40.5	22.3	11.1	-	-	20	−32.6	11.6	26.0	9.5
ECU05	Ignimbrite	2.776	79.237	Saraguro	Late Oligocene-Early Miocene (29.4 ± 2.6/19.0 ± 3.5)	-	6/10	R	220.3	0.9	14.4	18.3	-	-	20	42.7	14.4	−13.6	14.7
ECU06	Ignimbrite	2.775	79.248	Saraguro	Late Oligocene-Early Miocene (29.4 ± 2.6/19.0 ± 3.5)	140–21	10/10	N	15.6	−37.4	37.8	8.0	5.8	−24.0	20	8.3	7.1	9.4	7.3
ECU07	Ignimbrite	2.775	79.256	Saraguro	Late Oligocene-Early Miocene (29.4 ± 2.6/19.0 ± 3.5)	140–23	10/10	N	50.9	−39.0	197.1	3.4	33.2	−35.7	20	35.6	3.9	21.2	4.7
ECU08	Ignimbrite	2.759	79.403	Saraguro	Late Oligocene-Early Miocene (29.4 ± 2.6/19.0 ± 3.5)	340–26	10/10	N	2.6	−13.4	24.5	9.9	8.0	−37.0	20	10.3	9.9	22.5	8.6
ECU09	Ignimbrite	2.775	79.389	Saraguro	Late Oligocene-Early Miocene (29.4 ± 2.6/19.0 ± 3.5)	-	5/8	R	205.3	2.4	14.6	20.7	-	-	20	27.7	16.3	−12.1	16.6
ECU10	Ignimbrite	2.864	79.092	Saraguro	Late Oligocene-Early Miocene (29.4 ± 2.6/19.0 ± 3.5)	131–21	8/8	R	**206.9**	**38.8**	**47.3**	**8.1**	**193.0**	**31.1**	20	15.4	7.7	16.4	7.4
ECU11[a]	Ignimbrite	2.795	79.372	Saraguro	Late Oligocene-Early Miocene (29.4 ± 2.6/19.0 ± 3.5)	-	7/8	-	-	-	-	-	-	-	-	-	-	-	-
ECU12	Ignimbrite	2.842	79.123	Saraguro	Late Oligocene-Early Miocene (29.4 ± 2.6/19.0 ± 3.5)	-	7/8	N	12.5	−19.7	20.5	13.6	-	-	20	14.9	11.5	5.0	11.3
ECU13[a]	Lacustrine	2.756	78.894	Turi (Bilbian)	Late Miocene (14.7 ± 2.4/12.3 ± 1.6)	94–40	1/10	-	-	-	-	-	-	-	-	-	-	-	-

Tectonics

10.1029/2020TC006684

Table 1
Continued

Site	Lithology	Lat (°S)	Long (°W)	Unit in map 1:1.000.000 (1:50.000)	Age (Ma)	Bedding (dipdir -dip)	In-situ ChRM or HT						Tilt-corrected		Vertical-axis rotations				
							n/N	STATE	D (°)	I (°)	k (°)	α_{95} (°)	D (°)	I (°)	Pp (Ma)	R (°)	ΔR (°)	F (°)	ΔF (°)
ECU14	Lava	2.759	78.891	Turi/ Azogues Groups (Cojitambo)	Late Miocene (7.8 ± 0.8)	-	10/10	N	21.2	−0.5	15.9	12.5	-	-	10	23.1	9.9	9.6	10.1
ECU15	Lava	2.754	78.888	Turi/ Azogues Groups (Cojitambo)	Late Miocene (7.8 ± 0.8)	-	9/9	N	24.4	20.0	227.2	3.4	-	-	10	26.3	3.2	9.9	3.8
ECU16	Ignimbrite	2.936	78.956	Turi	Late Miocene (9.6 ± 1.8/8.0 ± 1.2)	-	9/10	N	342.9	−14.7	10.4	16.7	-	-	10	−15.2	13.6	4.2	13.3
ECU17	Ignimbrite	2.937	78.942	Turi	Late Miocene (9.6 ± 1.8/8.0 ± 1.2)	-	7/10	R	177.0	24.0	11.46	18.6			10	−1.1	16.0	13.6	14.7
ECU18	Ignimbrite	3.013	78.869	Chinchin	Middle-Late Eocene (42.8 ± 3.8)	-	7/10	R	176.2	33.3	25.0	12.3	-	-	40	−1.5	11.7	11.5	10.4
ECU19	Ignimbrite	3.003	78.846	Chinchin	Middle-Late Eocene (42.8 ± 3.8)	310–26	10/10	R	171.8	28.8	96.9	4.9	187.2	46.0	40	9.5	6.0	24.2	5.6
ECU20	Ignimbrite	2.939	78.935	Saraguro	Late Oligocene-Early Miocene	296–40	10/10	N	335.0	−7.1	203.9	3.4	346.7	−36.2	20	−10.9	3.9	21.3	4.7
ECU21[b]	Red Beds	2.973	78.910	Silante (Quingeo)	Middle-Late Eocene (42.8 ± 3.8)	135–34	9/10	N	**209.2**	**−40.5**	**6.2**	**29.1**	**239.6**	**−40.9**	-	-	-	-	-
ECU22	Lava	3.000	78.893	Chinchin	Middle-Late Eocene (42.8 ± 3.8)	-	9/9	R	210.5	10.1	100.7	5.2	-	-	40	32.8	4.7	−11.7	5.7
ECU23[a]	Ignimbrite	2.931	78.999	Turi	Late Miocene (9.6 ± 1.8/8.0 ± 1.2)	126–45	0/10	-	-	-	-	-	-	-	-	-	-	-	-
ECU24[a]	Ignimbrite	2.879	78.899	Turi	Late Miocene (9.6 ± 1.8/8.0 ± 1.2)	-	4/10	-	-	-	-	-	-	-	-	-	-	-	-
ECU25	Ignimbrite	2.824	78.856	Saraguro	Late Oligocene-Early Miocene (29.4 ± 2.6/19.0 ± 3.5)	-	10/10	N	65.9	−16.7	21.2	10.7	-	-	20	68.3	9.0	2.0	9.2
ECU26	Ignimbrite	2.826	78.828	Saraguro	Late Oligocene-Early Miocene (29.4 ± 2.6/19.0 ± 3.5)	-	7/10	N	**38.0**	**21.4**	**12.6**	**17.7**			20	40.6	15.0	6.1	14.3
ECU27[a]	Ignimbrite	2.840	78.800	Saraguro	Late Oligocene-Early Miocene (29.4 ± 2.6/19.0 ± 3.5)	-	10/10	-	-	-	-	-	-	-	-	-	-	-	-
ECU28	Ignimbrite	2.841	78.785	Saraguro	Late Oligocene-Early Miocene (29.4 ± 2.6/19.0 ± 3.5)	-	7/10	N	**347.6**	**−49.4**	**88.8**	**6.4**			20	−9.8	7.9	34.0	6.2

Site	Lithology	Lat (°S)	Long (°W)	Unit in map 1:1.000.000 (1:50.000)	Age (Ma)	Bedding (dipdir -dip)	In-situ ChRM or HT						Tilt-corrected		Vertical-axis rotations				
							n/N	STATE	D (°)	I (°)	k (°)	α_{95} (°)	D (°)	I (°)	Pp (Ma)	R (°)	ΔR (°)	F (°)	ΔF (°)
ECU29[a]	Ignimbrite	2.881	78.872	Saraguro	Late Oligocene-Early Miocene (29.4 ± 2.6/19.0 ± 3.5)	-	6/10	-	-	-	-	-	-	-	-	-	-	-	-
ECU30	Ignimbrite	3.004	78.822	Chinchin	Middle-Late Eocene (42.8 ± 3.8)	-	6/10	N	11.7	−23.4	11.2	20.9	-	-	40	14.0	18.0	1.6	16.8
ECU31[b]	Ignimbrite	3.001	78.808	Saraguro	Late Oligocene-Early Miocene (29.4 ± 2.6/19.0 ± 3.5)	-	9/10	N	80.8	−42.5	2.8	37.2	-	-	-	-	-	-	-

Note. The geographic coordinates are referred to WGS84 datum. The geological units are from the Mapa Geológico De La República Del Ecuador at scale 1:1.000.000 (2017), or from the available 1:50,000 Instituto Nacional De Investigación Geológico Minero Metalúrgico geological maps. Absolute dating ages are from Hungerbühler et al. (1995), Steinmann (1997), Steinmann et al., (1999), and Hungerbühler et al. (2002). "sub-hzt" indicate sub-horizontal bedding. n/N is number of samples giving reliable results/number of studied samples at a site. STATE indicate normal (N) or reversal (R) magnetization state. D and I are site mean declination and inclination calculated before and after tectonic correction for a characteristic magnetization component (ChRM) or high Temperature (HT; in bold) component; k and α_{95} are statistical parameters after Fisher (1953). Pp: Considered paleopoles age from Torsvik et al. (2012). Site mean rotation (R) and flattening (F) values, and relative errors ΔR and ΔF (according to Demarest (1983)) are relative to coeval D and I.

[a]Failed sites. [b]Rejected sites with values of $\alpha_{95} > 25°$.

(Figure 2). We collected middle-upper Eocene to Miocene ignimbrites (26 sites), Eocene and Miocene lavas (three sites), one site in upper Eocene red beds, and one site in upper Miocene lacustrine deposits (Table 1). Hungerbühler et al. (1995), Steinmann (1997), Steinmann et al. (1999), and Hungerbühler et al. (2002) dated the igneous lithologies and tephra layers interbedded in the sedimentary succession along the sampling area using apatite (AFT) and zircon fission tracks (ZFT) analysis, as listed in Table 1. In detail, we collected one site (ECU21) from the red beds of the Quingeo Fm., dated between 42.4 ± 4.4 and 34.9 ± 4.0 Ma with both AFT and ZFT dating (mid-late Eocene); four sites (three ignimbrites and one lava; ECU18, 19, 30, and 22, respectively) from the Chinchín Fm., dated with ZFT at 42.8 ± 3.8 Ma; 19 sites (ECU01-12, 25–29, and 31) from ignimbrites of the Saraguro Fm., dated with ZFT between 29.4 ± 2.6 and 19.0 ± 3.5 Ma (late Oligocene-early Miocene); and seven sites (ECU13-17, and 23–24) dated with both AFT and ZFT, from different lithologies of the upper Miocene Turi/Azogues Groups. Within these, the Cojitambo porphyritic lava dome (sites ECU14, 15) is dated to 7.8 ± 0.8 Ma (late Miocene); ash layers in between the sedimentary Biblián Fm. (ECU13) were dated to 14.7 ± 2.4 and 12.3 ± 1.6 (middle Miocene), and ignimbrites (ECU16,17, 23, and 24) of the Turi Fm. between 9.6 ± 1.8 and 8.0 ± 1.2 Ma (late Miocene).

A total number of 300 paleomagnetic samples were gathered at 31 sites (Figure 2 and Table 1). At each site, we drilled eight-ten cores using a petrol-powered portable drill cooled by water—except site ECU13 that was hand sampled in soft upper Miocene lacustrine sediments—and oriented them in situ using both a Sun and a magnetic compass, corrected for the local geomagnetic declination in September/October 2019 (~3°W according to NOAA's National Geophysical Data Center https://www.ngdc.noaa.gov/geomag/calculators/magcalc.shtml). The cores were then cut into standard paleomagnetic specimens of 22 mm height.

Paleomagnetic measurements were performed in a shielded room, using a 2G Enterprises direct current-superconducting quantum interference device cryogenic magnetometer. Alternating field (AF) demagnetization using three coils online with the magnetometer starting from 10 mT and reaching a maximum AF peak of 120 mT (10 mT steps until 80 and 20 mT steps afterward) was routinely used in 10 steps. Fifty-eight samples from six sites that were not demagnetized at 120 mT (Table 1), and samples from site ECU21, were thermally cleaned using a Pyrox shielded oven in 10 steps up to 690°C.

Demagnetization data were plotted on orthogonal vector component diagrams (Zijderveld, 1967), and principal component analysis was used to isolate magnetization components (Kirschvink, 1980). Site-mean paleomagnetic directions were computed using Fisher (1953) statistics and plotted on equal-area projections, using the Remasoft software. Paleomagnetic rotation and flattening values with respect to the South America plate were calculated according to Demarest (1983), using reference paleo-poles from Torsvik et al. (2012). Rotations were calculated for both site-mean (Table 1) and locality-mean directions. Mean ages of the sampled rocks as derived from absolute and/or relative dating available from the literature were used to select the corresponding age paleopoles (Table 1).

The magnetic mineralogy was investigated for one sample per site by thermo-magnetic curves performed by an AGICO MK1-FA Kappabridge. The magnetic susceptibility of a powdered sample per site was measured in a heating-cooling cycle from room temperature up to 700°C.

We mostly sampled volcanics that are expected to record the paleo secular variation (PSV) of the geomagnetic field, and therefore to yield paleomagnetic directions more scattered than those from sediments. This represents a potential error source

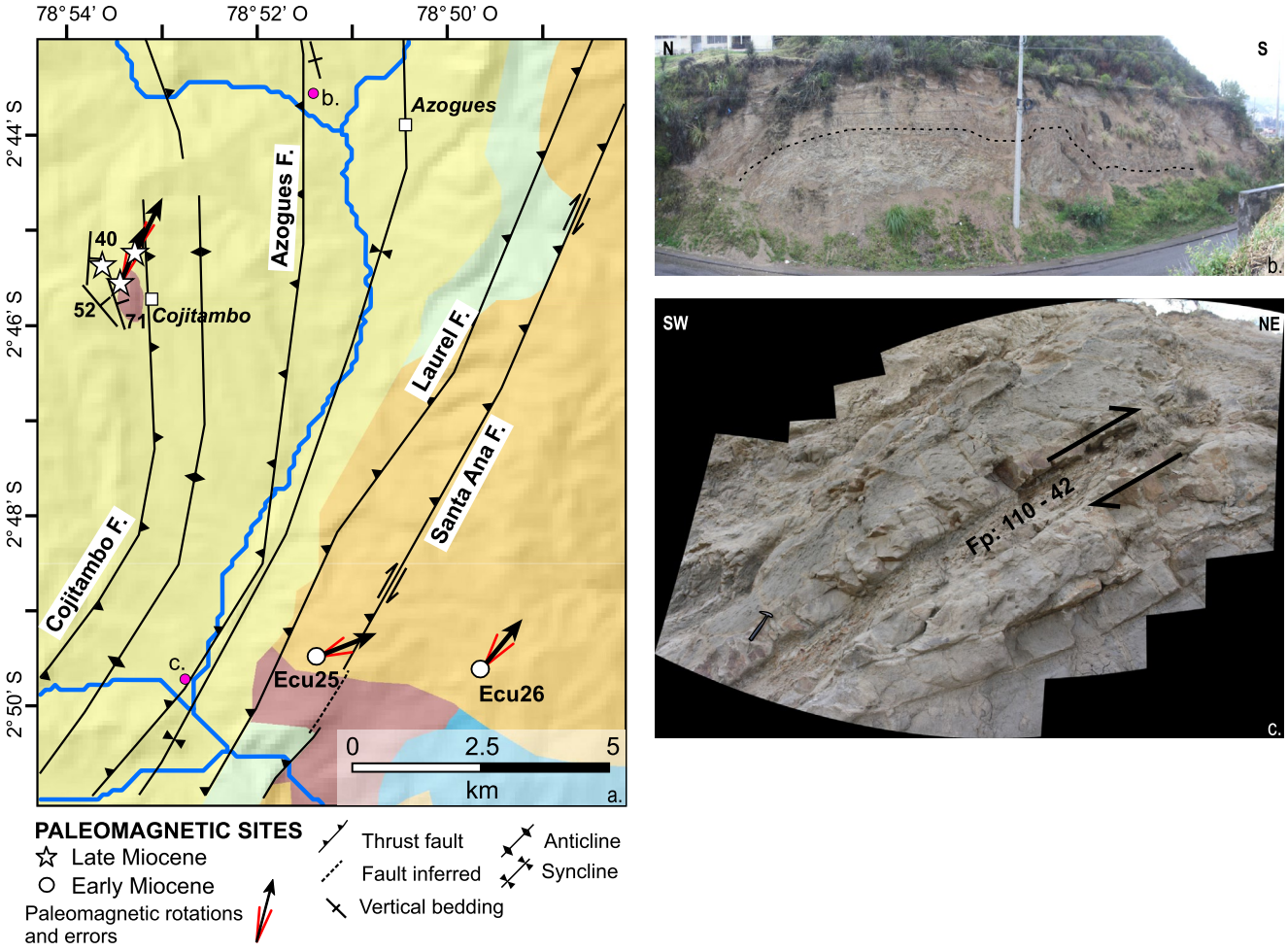

Figure 4. Detail of field observations along the Interandean Valley. (a) Close-up geologic map of the northern part of the studied area (see Figure 2 for geologic reference). Pink circle shows the location of field pictures in panels (b and c). Compressive deformation is well apparent through eastward increasing layer dip West of the Cojitambo Fault. Folding (4b) and vertical strata are also observed east of the Azogues fault. Thrust faulting along the Azogues fault of the continental Miocene succession is exposed along the main valley (4c). Geologic hammer to the left of the fault is for scale.

for data interpretations in terms of tectonic rotations (e.g., Merrill et al., 1996). Therefore, following the method of Deenen et al. (2011) that considers the virtual geomagnetic pole (VGP) distribution and the relative statistical precision parameter K and A95 as a function of N (number of observations), we tested the PSV averaging of both site-mean and locality-mean paleomagnetic datasets (Tables S1 and S2). A95 values were obtained from Fisher statistics on VGPs calculated from magnetization components from specimens gathered in each site (site-mean A95), and given belt sectors (locality-mean A95).

Mean inclinations from data groups of the same age were used to calculate paleolatitudinal values.

4. Results

4.1. Paleomagnetism and Evaluation of Latitudinal Drift

Scattered or erratic demagnetization diagrams were observed at seven sites that were excluded from further considerations (Table 1). In the remaining 24 sites, a viscous component was removed at 20 mT or 300 °C (Figure 5). In the AF-cleaned sites, a characteristic magnetization component (ChRM) was isolated in the 20–120 mT field interval (Figure 5a–5d). In the thermally cleaned sites, a high-temperature (HT) component was identified in the 400–690°C temperature range (Figure 5e–5g). ChRMs and HT components were used to calculate site-mean paleomagnetic directions.

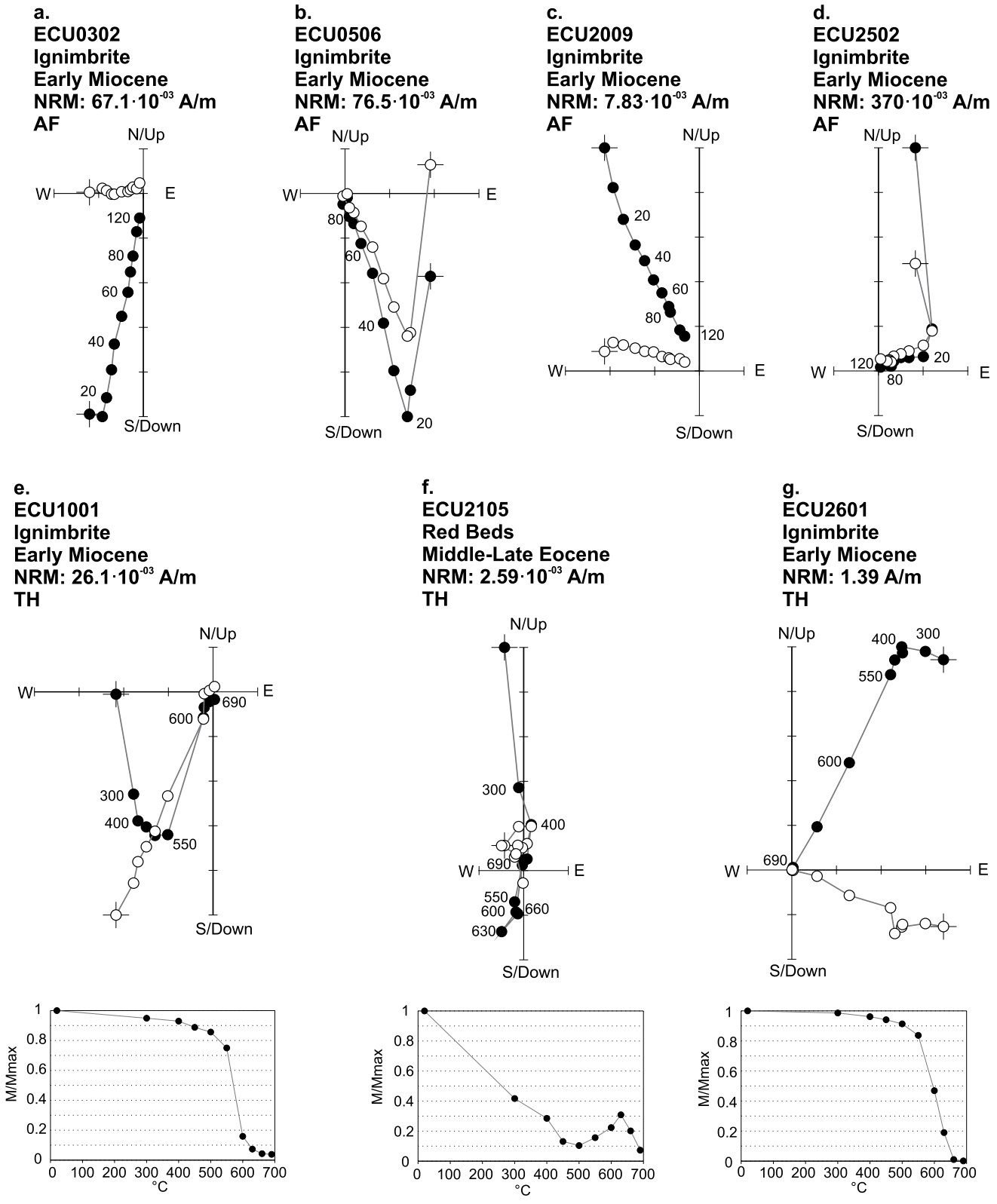

Figure 5. Orthogonal vector diagrams of typical demagnetization data, in-situ coordinates. Solid and open circles represent projection on the horizontal and vertical planes, respectively. Demagnetization steps are in mT for alternating field (AF) and in °C for thermal (TH) demagnetization data. Normalized intensity of magnetization versus temperature graphs are reported for thermally treated samples.

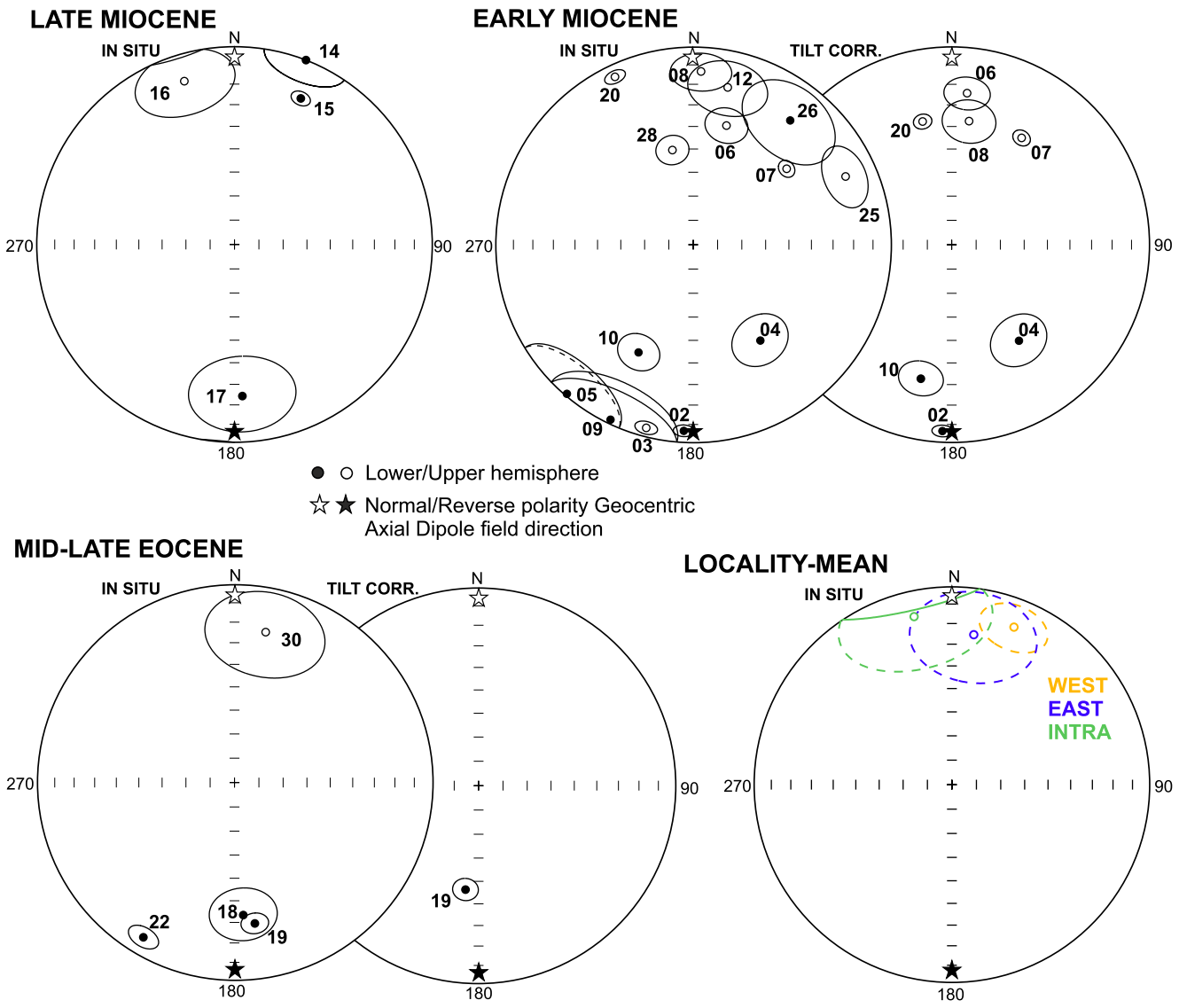

Figure 6. Equal area projection of the site-mean paleomagnetic directions from the study area, grouped by age. In-situ locality mean directions are also shown (see text). Solid and open circles represent projection on the lower and upper hemisphere, respectively. Light-gray circles are the projection of the α_{95} confidence cones.

Thermomagnetic curves (Figure S1 in supporting information) show predominantly 550–600°C Curie temperatures, in some cases associated with minor susceptibility drop at 250°C. Demagnetization diagrams together with thermo-magnetic curves suggest magnetite and subordinate titano-magnetite (or pyrrhotite at sites ECU08, 17, and 22) as main magnetic carriers, along with hematite at the seven thermally demagnetized sites (ECU05, 10, 15, 21, 26, 28 and 31).

The α_{95} values relative to the site-mean paleomagnetic directions vary from 3.2° to 20.9°, 10° on average, whereas sites ECU21 and ECU31 that exceed a 25° α_{95} threshold value were discarded. The reliability of few sites showing α_{95} values ranging from 18° to 21° is supported by a comparison of their A95 values with validity limits by Deenen et al. (2011) that will be discussed below. The reliable sites show both normal (12 sites) and reverse (10 sites) polarity states (Figure 6 and Table 1).

The inclination-only (Arason & Levi, 2010) fold (McFadden, 1990), and reversal (McFadden & McElhinny, 1990) tests—performed on both the entire data set and on groups of similar age sites—are indetermi-

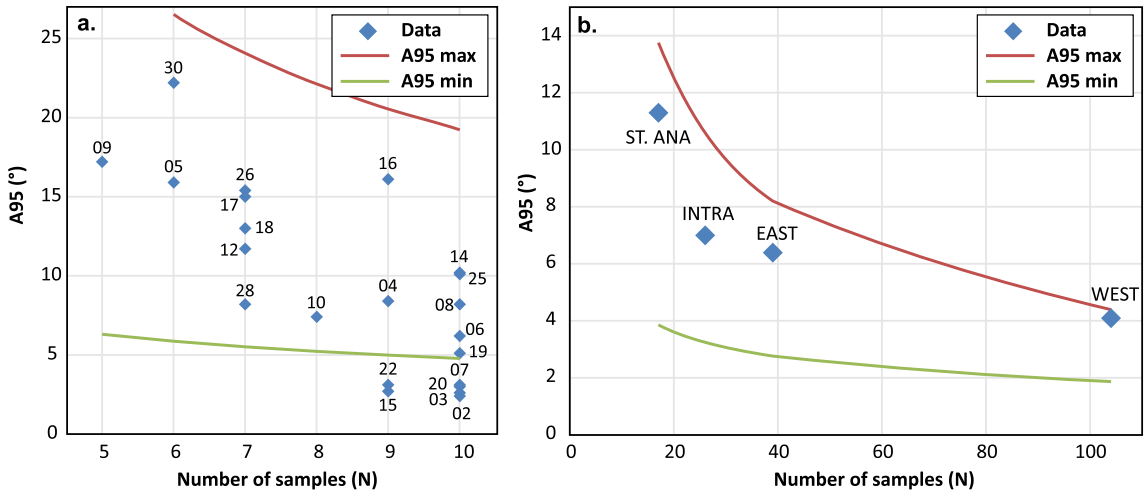

Figure 7. Deenen et al. (2011) reliability paleo secular variation (PSV) averaging criteria for (a) site-mean and (b) locality-mean paleomagnetic datasets. Most of the site are PSV averaged. Considering the locality-mean dataset all of the data do average the PSV.

nate (Tables S3–S5 in supporting information). However, the magnetic mineralogy is mostly dominated by magnetite, the occurrence of directions acquired on both polarity states, the spread of both in situ and tilt corrected paleomagnetic directions, and their distance from the local (normal- and reverse-polarity) geocentric axial dipole field directions (Figure 6) imply no magnetic overprint and support the primary nature of the isolated ChRMs and HT components.

Reverse-polarity directions with southerly declinations were inverted to normal polarity before performing a directional analysis of site groups from given sectors of the chain.

Considering both in-situ and tilt-corrected sites to the west of the Azogues fault (ECU02-10; 12; 14–15 in Figure 2), the resulting mean direction is defined as $D = 18.4°$, $I = -12.3°$ ($\alpha_{95} = 12.6°$). However, to avoid mixing in-situ and tilt-corrected sites we rely on the in-situ population only, yielding a mean direction given by $D = 21.5°$, $I = 15.9°$ ($\alpha_{95} = 11.6$; Figure 6). This is used to evaluate the regional rotation pattern of the Cordillera Occidental (group "WEST" in supplementary tables and Figures 6 and 7b).

To the E of the Azogues fault, most of the directions are in in-situ coordinates, except for sites ECU20 and ECU19. However, tilt-corrected direction from site ECU20 and in-situ directions from nearby (2.5 km) site ECU17 and ECU16 are similar (Figure 6) and yield an average direction defined by $D = 350.9°$, $I = -25.2°$, and $\alpha_{95} = 22.5°$. Considering only in-situ coordinates the average direction obtained is $D = 347.3°$, $I = -14.4$, $\alpha_{95} = 25.4°$ (group "INTRA" in Figures 6 and 7b, and in the supplementary tables). The ages of these sites range from the Late Oligocene to the Late Miocene. Further east, tilt-corrected direction from site ECU19 and in-situ directions from sites ECU18, ECU22, and ECU30 are somehow scattered, and if averaged together provide a direction defined by $D = 12.4°$, $I = -28.8°$, and $\alpha_{95} = 23.1°$. Considering only in-situ values, the average direction is defined by $D = 8.3°$, $I = -24.7$, and $\alpha_{95} = 22.1°$ (group "EAST" in supplementary tables and Figure 7b). Finally, the nearby in-situ directions from sites ECU25 and ECU26 are consistently NE-ward directed (group "St. Ana" in supplementary tables and Figure 7b), whereas site ECU28 is far from other sites and yields an NW-ward in-situ direction.

The results of the Deenen et al. (2011) PSV averaging test show that most of the site-mean paleomagnetic directions do average the PSV, falling in between the lower and upper-reliability boundaries (Figure 7a and Table S1). The A95 from only six sites (ECU02, 03, 07, 15, 20, and, 22) are located below the lower boundary, suggesting no PSV averaging. This result is somehow surprising, as volcanic sites drilled in single volcanic units should record a snapshot of geomagnetic field direction thus are expected to systematically not average the PSV. We conclude that in the majority of our volcanic sites we sampled, in fact, multiple volcanic units (i.e., multiple pyroclastics flows from the same formation) where PSV is averaged out. Sites were

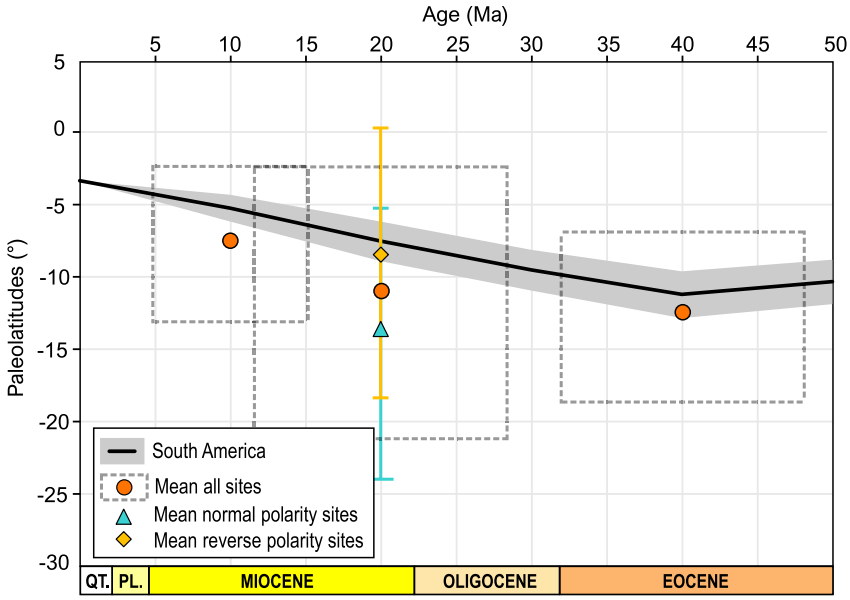

Figure 8. Expected paleolatitudes at Cuenca (2° 54′S; 79° 0′W) from 50 Ma to present considering South America paleomagnetic poles listed by Torsvik et al. (2012) are shown as black lines within the gray area (α_{95} ranges around mean inclinations). Paleolatitudes from mean paleomagnetic inclinations relative to each rock age group are shown as orange circles. Additional reverse and normal polarity site-mean paleolatitudes are given with relative error for the Early Miocene data, for which we have the highest number of sites. Dashed boxes are paleolatitude and age uncertainties.

spread across different scattered outcrops, and the results of the Deenen et al. (2011) test imply that such outcrops frequently represented multiple volcanic units. Boundaries of single volcanic units may have been poorly apparent due to the strong welding of the sampled ignimbrites that frequently appeared as massive bodies lacking internal sedimentological features.

When sites are grouped in structurally homogeneous domains (i.e., no main fault occurs between them), the locality-mean directions show a complete PSV averaging (Figure 7b and Table S2), showing that our data can be used to assess tectonic rotations. Moreover, several works in the past proved that orogenic rotations can be evaluated by paleomagnetic data from volcanic rocks, provided that a sufficiently high number of data are averaged out (e.g., Andreani et al., 2014; Gattacceca et al., 2007; Hernandez-Moreno et al., 2014, 2016; Pellegrino et al., 2018; Piper et al., 1997; Márton et al., 2006; Siravo et al., 2020, among many others).

The sampled ignimbrites are welded (Chiaradia et al., 2004; Mulas et al., 2017) that suggest high-emplacement temperatures (e.g., Branney et al., 1992; Cas & Wright, 1987; Ekren et al., 1984; Friedman et al., 1963; McClelland et al., 2004; Riehle, 1973; Riehle et al., 1995; Yagi, 1966). In such cases compaction occurs soon after emplacement and at high temperatures (Quane et al., 2009), frequently higher than the magnetite Curie temperature (580°C; Bleil & Petersen, 1982). Thus we expect that the sampled ignimbrites faithfully recorded the local geomagnetic field inclination after emplacement, excluding the occurrence of sedimentation-flattening processes that usually bias paleo-inclination values in sediments (e.g., Arason & Levi, 1990). This implies that the paleo-inclinations from our dataset can be safely used to evaluate possible latitudinal drift parallel to the orogen that was claimed in the past for Jurassic red-beds of the Eastern Cordillera of Colombia (Bayona et al., 2006), and for the upper Cretaceous oceanic terranes of Ecuador (Lapierre et al., 2000; Reynaud et al., 1999) and Colombia (MacDonald & Opdyke, 1972).

Paleo-inclinations systematically document a southern hemisphere provenance (Figure 8), but, when compared to expected South American values, no significant difference exists, suggesting that the sampled volcanic locations remained virtually stable with respect to the South America margin.

5. Rotation Pattern and Tectonic Implications

Site-mean rotation values calculated using in-situ and tilt-corrected coordinates with respect to South America are both counterclockwise (CCW) and CW in sense, varying from −32° to 68° (Figure 2; Table 1; Figure S2 in supporting information). Locality-mean in-situ directions are used to evaluate regional rotation patterns. A rather uniform 23.9° ± 9.6° CW rotation (R) pattern characterizes the domain W of the Azogues fault, which includes the western Interandean Valley, the Cajas Plateau of the Cordillera Occidental, and the Pallatanga fault zone (Figures 2 and Figure S2). Here, the uniquely CCW-rotated site ECU04 is considered an outlier and discarded. To the E of the Azogues fault, sites ECU16, 17, and 20 are on average not rotated ($R = -10.8° \pm 20.5°$). Sites ECU18, 19, 22, and 30 from along the Peltectec Fault provide a non-significant rotation $R = 9.9° \pm 19.1°$. Sites ECU25, 26, straddling the Santa Ana dextral fault, are rotated CW by 68° ± 9.0° and 40° ± 15.0°, respectively. Finally, site ECU28 is far from any other site to infer a reliable rotation pattern and will not be considered onward (Figures 2 and S2).

5.1. Paleomagnetic Assessment of Post-Mid Eocene Strike-Slip Fault Offset

There is wide evidence that—in the vicinity of major strike-slip faults—the paleomagnetic pattern is characterized by rotated crustal blocks and secondary strike-slip faults separating them (e.g., McKenzie & Jackson, 1986; Ron et al., 1984; Sonder et al., 1994, among many others). It has been shown that—if a quasi-continuous crust deformation model is assumed—the width of the rotation-deformation zones adjacent to the faults and the maximum rotation values are proportional to strike-slip offset, thus can be used to estimate the significance of the faults themselves (Lamb, 1987; Nelson & Jones, 1987; Sonder et al., 1994). Major continental strike-slip faults with offsets of some tens of km (or more) were shown to generate a 10–20 km wide damage rotation zone on each fault side, with CW (CCW) rotations exceeding 90° in case of dextral (sinistral) faults (e.g., Hernandez-Moreno et al., 2014, 2016; Pellegrino et al., 2018; K. Randall et al., 2011; Siravo et al., 2020; Sonder et al., 1994; Speranza et al., 2018).

Concerning our data set, four sites straddling the Peltectec fault (ECU18, 19, 22, and 30) are scattered and on average show no rotation ($R = 9.9° \pm 19.1°$). Similarly, site ECU08, located in between the Pallatanga fault system shows a small 10° rotation, while the 28° ± 16° CW rotation of site ECU09 at 1 km from the fault is not significantly different from the regional 24° ± 10° CW rotation of the Cordillera Occidental. Nevertheless, a Quaternary-Holocene dextral strike-slip offset along the Pallatanga fault is reported (Winter & Lavenu, 1989; Winter et al., 1993). However, the Holocene displacements values estimated by Winter et al. (1993) (from 27 ± 11 m to 960 ± 70 m) translate to a barely detectable maximum paleomagnetic rotation ranging from 3° to 6°, when the formula of Lamb (1987) and widths of the deformation-rotation zone of 5, 10, and 20 km are assumed (e.g., Hernandez-Moreno et al., 2014; Pellegrino et al., 2018). Our data provide no evidence for a paleomagnetically-detectable offset along the Peltectec and Pallatanga fault systems after Middle Eocene and Early Miocene respectively, confirming previous suggestions that the accretion of oceanic terranes to the western Ecuador margin was completed by Late Cretaceous times (Luzieux et al., 2006; Spikings et al., 2010; Vallejo et al., 2009, 2019).

Conversely, a dextral fault displacement may be inferred considering the systematic CW rotations observed at sites ECU25 and 26, which are located up to 3 km from the Santa Ana fault, for which both reverse and dextral displacements were suggested (Hungerbühler et al., 2002). Again, by using the formula by Lamb (1987) and considering 68° as the maximum rotation angle and 6 km as the width of the rotation domain (including both sides of the fault), we infer a 14 km offset for the Santa Ana fault. Although only two sites are obviously not enough to solidly constrain fault displacement, it is clear that this is not a major transcurrent feature of the Andes, as sites ECU16, 17, and 20, located 15 km further south and a few km W of the fault are not rotated ($R = -10.8° \pm 20.55°$; Figure 2).

We conclude that strike-slip induced-rotations are almost absent in the study area. Such evidence is indeed consistent with the paleo-latitude data of Figure 8 that shows no significant difference from South America's expected values. Thus our data exclude the occurrence in the Ecuadorian Andes of terranes undergoing latitudinal drift and therefore indicate no significant orogen-parallel strike-slip activity, at least since mid-late Eocene (~40 Ma).

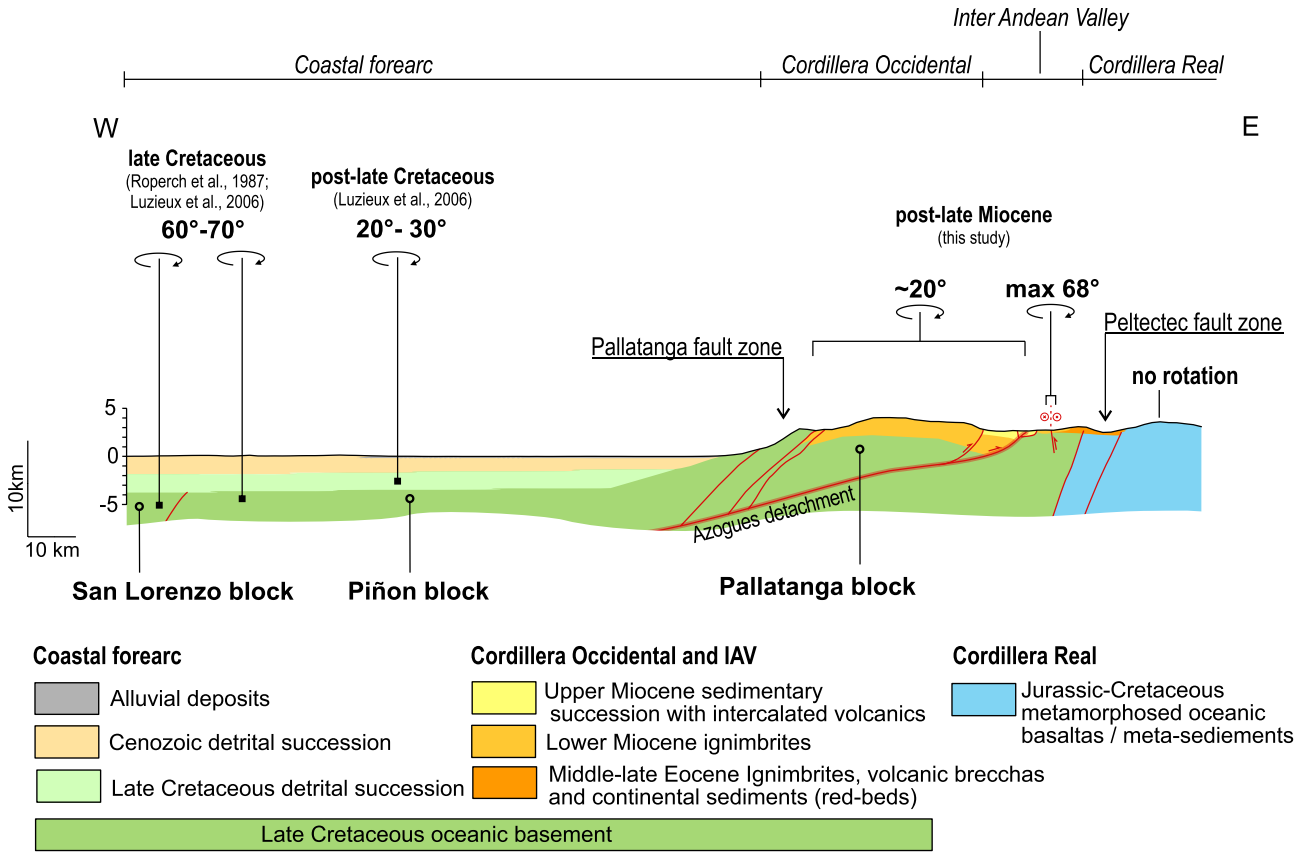

Figure 9. Schematic geologic cross-section of the southern (lat ~2°S) Ecuadorian Andes (location in Figure 1c) and paleomagnetic rotations with respect to South America considering our data and those by Roperch et al. (1987) and Luzieux et al. (2006). See text for explanation.

5.2. CW Rotation of the Cordillera Occidental and Genesis of the Interandean Valley

The Cajas Plateau and the western Interandean Valley, West of the Azogues fault, underwent a 24° ± 10° CW rotation whereas a non-rotating domain occurs to the east (Figure 2). Broadly similar paleomagnetic rotation values were documented over the same rotational thrust sheet, contrasting with adjacent non-rotated foreland domains (e.g., Channell et al., 1990; Cifelli & Mattei, 2010; Maffione et al., 2009; Oldow et al., 1990; Shaanan et al., 2015; Speranza et al., 2018; Weil et al., 2010). For instance, Channell et al. (1990), Oldow et al. (1990), and Speranza et al. (2018) showed that—although strike-slip faults occur in the Sicilian fold and thrust belt—high-magnitude and rather constant CW paleomagnetic rotations may be better explained by rotational nappe emplacement. In the Bolivian Orocline of central Andes, rotations of opposite sign at orocline limbs have been interpreted as also related to nappes displaced and rotating above deep-seated crust detachments (Barke et al., 2007; Butler et al., 1995; Isacks, 1988; MacFadden et al., 1995; Maffione et al., 2009; Rousse et al., 2003).

The sites from the Cajas Plateau are far from any surface fault, besides the Pallatanga fault. However, our data suggest a lack of post early Miocene strike-slip deformation. Compressive deformation is conversely documented in the upper Miocene sediments exposed in the vicinity of the Cojitambo and Azogues faults (Figure 4).

The age of nappe emplacement-related CW rotation and the onset of Interandean Valley continental sedimentation also coincide suggesting a genetic link between the two processes. Continental deposition in the Cuenca area started in the Middle-Late Miocene (first continental deposits were dated at 12.1 ± 1.2 Ma by Steinmann et al., 1999), while CW rotation is constrained to the Late Miocene (younger rotated data are from the Cojitambo lava dome, dated at 7.8 ± 0.8 Ma by Steinmann et al., 1999). Therefore, we infer that after the Late Miocene times the Cajas Plateau and the Cordillera Occidental were carried on top

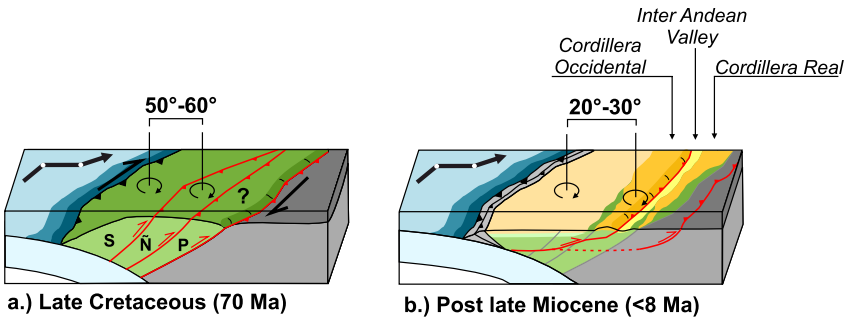

Figure 10. Evolutionary block diagram. (a) Caribbean-plate affinity oceanic blocks collided with South America with an average dextral displacement, and rotated 50–60° CW at end of Cretaceous. (b) Mid-crustal detachment accommodated 20–30° CW rotation in the Cordillera Occidental and Coastal Forearc, after the late Miocene. Black thick line show the Nazca plate convergence vector from ~70 Ma to present (Pardo-Casas & Molnar, 1987). Direction changes (white spots) occured at 26 and 20 Ma.

of a mid-crustal rotational detachment whose front coincides with the Azogues fault in the Interandean Valley (Figure 9). We also propose that Interandean Valley developed as a relatively narrow flexural basin in front of the advancing Cordillera Occidental deformation front and was subsequently involved in the compression by foreland propagating thrust faults (Figure 9), consistently with previous interpretations by Hungerbühler et al. (2002), Lavenu et al. (1995), and Steinmann et al. (1999), and that deformation likely continued through the Pliocene. Elongated sedimentary basins lying on deformed orogens in front of thrust sheets and acting as sediment depocenters for a few million years are observed further south in the Andes (Sierra Pampeana; e.g., Strecker et al., 1989) and in Tibet (e.g., Mula basin; Todrani et al., 2020). On the other hand, classical foreland basins of orogenic fronts are hundreds of km wide and may contain huge packages of turbidites thousands of meters thick (e.g., Davis et al., 1996).

East of the Interandean Valley, the lack of significant CW rotation excludes any post-Eocene strike-slip displacement along the Peltectec fault that marks the suture zone between the Cordillera Occidental and Cordillera Real blocks (Figure 9). This conclusion is partly inconsistent with previous studies that, relying on thermochronologic data from the Cordilleras Occidental and Real, suggest Eocene tectonic oblique-slip reactivations within specific fault-bounded massifs (Spikings et al., 2001, 2005, 2010). The alternative hypothesis is that strike-slip shear along the Peltectec fault pre-dated the Mid-Late Eocene sites paleomagnetically sampled by us.

Our data yield the first paleomagnetic constraints to the rotational pattern of the Cordillera Occidental and Real of Ecuador; however previous upper Cretaceous paleomagnetic data from the Coastal forearc investigated the deformation history of the oceanic blocks that represent the crystalline basement of Ecuadorian Andes from the forearc to the Interandean Valley (Luzieux et al., 2006; Roperch et al., 1987). We recalculated the paleomagnetic rotations with respect to the South American margin comparing the combined data set by Roperch et al. (1987) and Luzieux et al. (2006) with updated plate reference poles by Torsvik et al. (2012) (Figure 1c; Table S6 in supporting information). We find that the oceanic basement formations (Piñon and San Lorenzo; late Turonian - Coniacian) and the younger detrital Cayo formation (Santonian–Maastrichtian) yield CW rotation values of 66° ± 17° and 28° ± 9°, respectively. A 40°–50° CW rotation and complete incorporation of the Caribbean-related oceanic blocks to the South American margin at 70 Ma was suggested by Luzieux et al. (2006) (Figure 10a), but no explanation was given for the remaining 28° ± 9° post-Cretaceous rotations.

Here we stress that the 28° ± 9° post-Cretaceous CW rotation of the Coastal forearc is statistically indistinguishable from the 24° ± 10° Neogene CW rotation documented by us in the Cordillera Occidental and Interandean Valley. Thus we argue for a Neogene age of the CW rotation documented by Luzieux et al. (2006) in uppermost Cretaceous strata from the Coastal forearc (Figure 10b).

We suggest that a mid-crustal rotational detachment lying below both the Coastal forearc and the Cordillera Occidental, emerging along the Interandean Valley, would explain the paleomagnetic data set from the oce-

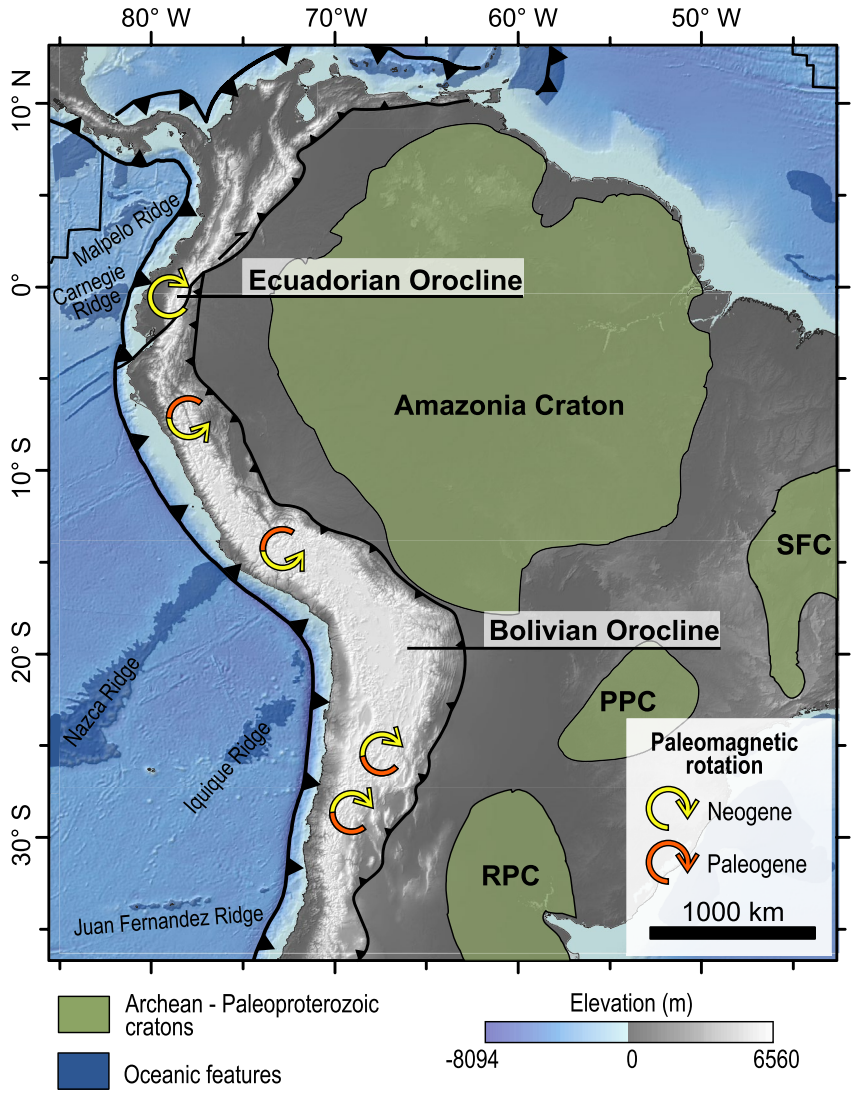

Figure 11. Continental-scale paleomagnetic rotation pattern along the Andes with respect to South America. Cenozoic paleomagnetic rotations coincide with the Nazca trench and Andean chain reentrant-salient sequence and closely mirrors the occurrence and boundaries of South America cratons made by stiff Archean-Paleoproterozoic crust. In particular, what we call here "Ecuadorian Orocline" mimics the western boundary of the Amazonian Craton, which would have acted as foreland indenter for the Andean chain. SF: Sao Francisco Craton; PPC: Paranapanema Craton; RPC: Rio de la Plata Craton.

anic terrains of Ecuador (Figures 9 and 10b). The Late Miocene-Pliocene emplacement of such a regional rotational tectonic nappe is in agreement with both an Early-Late Miocene shortening event reported from the Cordillera Occidental, the Interandean valley, and the Oriente foreland basin (Baby et al., 2013; Roddaz et al., 2010; Spikings et al., 2010; Steinmann et al., 1999).

6. The Genesis of the Andean Orogenic Bends: From the Bolivian to the Ecuadorian Orocline

Our results show that thrust tectonics prevailed over strike-slip displacement in the southern Ecuadorian Andes during the late Cenozoic times. In a continental-scale framework, such a pattern is consistent with tectonics and paleomagnetic rotations observed from 30°S (northern Chile) to 5°S (Bolivia and Peru) along the Andean chain (Figure 11). The shape of both the subduction trench and the Andean chain is

characterized by orogenic salients and reentrants (e.g., Macedo & Marshak, 1999). Moving northward from 30°S, the Nazca trench forms an eastward sharp reentrant at ~20°S, which coincides with the "Bolivian Orocline" or "Arica deflection" of the Andes. Several paleomagnetic works showed that such orogenic feature might be related to different tectonics, such as a thrust-related bending ("saloon door" opening) (e.g., Isacks, 1988; MacFadden et al., 1995; Müller et al., 2002), slip partitioning due to oblique convergence (Abels & Bischoff, 1999; Arriagada et al., 2000, 2003; D. E. Randall et al., 1996), compression-related block faulting, lateral ramps accommodating panels of different shortening rates (Arriagada et al., 2008; Prezzi & Alonso, 2002; Prezzi & Vilas, 1998; Somoza et al., 1996), or the lateral expansion of the plateau driven by thickened crust spread similarly to the Tibetan Plateau (Maffione et al., 2009; Riller & Oncken, 2003). The deformation-related rotations started during early deformation stages (Puigdomenech et al., 2020; late Cretaceous-Paleocene) but mostly occurred during Late Eocene - Oligocene and Miocene times (Arriagada et al., 2008; Beck et al., 1994; Butler et al., 1995; Lamb, 2001a, 2001b; Maffione et al., 2009; Narea et al., 2015; Prezzi et al., 2004; Riller & Oncken, 2003). The apex of the Bolivian Orocline also coincides with the remarkable plateaus of Puna and Altiplano, characterized by high (4,000–5,000 m) topography, volcanism, and thick (75 km; Yuan et al., 2000) crust overlain by a hot, weak, and likely partially molten shallow crust layer. Shortening also peaks at maximum values at the Bolivian Orocline apex with respect to adjacent orogenic limbs (e.g., McQuarrie, 2002).

Further north, from 10°S to 5°N the Nazca trench bends westward forming a wide sub-circular salient that we call "Ecuadorian Orocline" (Figure 10). CCW rotations between 15°S and 5°S (Peru) were interpreted as marking the northern limb of the Bolivian oroclinal bend (Butler et al., 1995; Gilder et al., 2003; Roperch & Carlier, 1992; Rousse et al., 2005). Our data from the Cordillera Occidental of Ecuador fit in this regional salient-reentrant sequence, as the orogenic trend changes from N20°W to N20°E at ~4°S, and Neogene CW rotations are consistently observed north of 4°S. In this framework, the along-chain rotation pattern mimics the reentrant—salient sequence of the Andes, and the CCW rotations documented in Peru (15°–5°S) would characterize the shared limb of a Bolivian orogenic reentrant and an Ecuadorian salient (Figure 10).

Several geodynamic processes were claimed as major driving forces to explain the Bolivian Orocline formation and the related topographic expression: (a) strong influence from the underlying subducting Nazca plate (Capitanio et al., 2011), (b) shear stress and friction at the subduction interface (Iaffaldano & Bunge, 2008; Sobolev & Babeyko, 2005; Yáñez & Cembrano, 2004), (c) sub-lithospheric mantle flow (Russo & Silver, 1996; Wdowinski et al., 1989), (d) relative plate convergence (Pardo-Casas & Molnar, 1987) and (e) climate-driven surface processes (Lamb & Davis, 2003; Montgomery et al., 2001).

By adding further geodynamic suggestions on the formation of Andean orogenic bends, we highlight here the outstanding coincidence between the reentrant-salient chain sequence and the Amazonian Craton outline (Casquet et al., 2012; Figure 11). The inland advance of the Bolivian orocline reentrant coincides with a local lack of stiff cratonic areas east of the accretionary front, whereas the Ecuador salient perfectly encircles the Amazonian Craton boundaries. Thus, the Amazonian Craton may have represented a strong crustal indenter guiding the deformation distribution along the northern Andean belt. We infer that the stiff Archean-Paleoproterozoic core of northeastern South America has forced the Andean orogen to bend around it, whereas the Bolivian Orocline may arise from greater penetration within the continent allowed by a lack of Archean–Paleoproterozoic cratons east of the accretionary front (Figure 11).

7. Conclusions

We provide the first paleomagnetic dataset from the Cordillera Occidental, Interandean Valley, and the Cordillera Real of southern Ecuador. The data show a lack of significant strike-slip deformation along the Pallatanga and Peltectec faults after the Early Miocene and Middle Eocene, respectively, strengthening the suggestion that collision of Caribbean-related oceanic terrains with the Ecuadorian margin ended in the Late Cretaceous, at ca. 70 Ma (Luzieux et al., 2006). Eocene-Miocene paleo-inclinations from volcanic data reveal a southern hemisphere provenance but also paleo-latitudes systematically consistent with those expected for the South American plate, arguing firmly against post-Eocene northward terrane displacement in Ecuador.

A remarkably consistent CW rotation pattern of 20°–30° in the Cajas Plateau and the western Interandean Valley, suggests that the Cordillera Occidental emplaced over the non-rotating Cordillera Real as a rotational nappe after the Late Miocene. By considering the age consistency of paleomagnetic rotation and continental deposition onset along the Interandean Valley, we suggest that thrusting is the main cause of tectonic depression genesis. We interpret the Interandean Valley as a narrow flexural basin, formed ahead of a Cordillera Occidental thrust sheet and subsequently incorporated in the deformation, and we suggest that the main rotational thrust front corresponds to the Azogues fault, overlying a non-rotational thrust fault footwall.

The re-evaluation of data by Roperch et al. (1987) and Luzieux et al. (2006) yields a 28° ± 9° CW post-Cretaceous rotation of the Coastal forearc oceanic blocks with respect to South America that is, indistinguishable from the 24° ± 10° CW Neogene rotation documented by us in the Cordillera Occidental and west Interandean Valley. Thus we argue for a Neogene 20°–30° CW rotation of the whole western Andean chain of Ecuador, implying that the Azogues fault is the front of a mid-crustal rotational detachment underlying the entire Cordillera Occidental and Coastal Forearc of southern Ecuador.

Paleomagnetic evidence from Ecuador reveals that the Northern Andean Block—shown to be currently extruded NE-ward by GPS data—is a very recent feature of the northern Andes that has not accumulated a paleomagnetically-detectable displacement.

Finally, we note that the orogenic reentrant-salient sequence of the Nazca trench-Andean chain (and related Cenozoic paleomagnetic rotations) from northern Chile to Ecuador mimics closely the margin of the Archean–Paleoproterozoic Amazonian Craton and other minor cratons of South America. We infer that the stiff crust of the Amazonian Craton behaved as a foreland indenter, hampered inland deformation propagation, and caused the formation of what we call the "Ecuadorian Orocline", arisen by opposite-sign nappe rotations around the Craton apex.

Data Availability Statement

The paleomagnetic data supporting this work are available via Zenodo (Siravo, 2021; https://10.5281/zenodo.5040097).

Acknowledgments
The authors thank the Parque Nacional Cajas to allow the paleomagnetic sampling in the natural reserve (research permit N° 206-2019-DPAA/MA; project Paleomagnetismo, representative Maurizio Mulas). The authors also thank the local inhabitants of San Felipe De Molleturo village for the thrilling experience they kindly offered to us. Detailed comments by four anonymous reviewers, the Associate Editor, and the Editor Laurent Jolivet helped us to strengthen data statistical treatment and better focus on the geological implications of paleomagnetic rotations.

References

Abels, A., & Bischoff, L. (1999). Clockwise block rotations in northern Chile: Indications for a large-scale domino mechanism during the middlelate Eocene. *Geology*, *27*, 751–754. https://doi.org/10.1130/0091-7613(1999)027<0751:CBRINC>2.3.CO;2

Aizprua, C., Witt, C., Johansen, S. E., & Barba, D. (2019). Cenozoic stages of forearc evolution following the accretion of a sliver from the late cretaceous-Caribbean Large Igneous Province: SW Ecuador-NW Peru. *Tectonics*, *38*(4), 1441–1465. https://doi.org/10.1029/2018tc005235

Alvarado, A., Audin, L., Nocquet, J. M., Jaillard, E., Mothes, P., Jarrín, P., et al. (2016). Partitioning of oblique convergence in the Northern Andes subduction zone: Migration history and the present-day boundary of the North Andean Sliver in Ecuador. *Tectonics*, *35*(5), 1048–1065. https://doi.org/10.1002/2016tc004117

Alvarado, A., Audin, L., Nocquet, J. M., Lagreulet, S., Segovia, M., Font, Y., et al. (2014). Active tectonics in Quito, Ecuador, assessed by geomorphological studies, GPS data, and crustal seismicity. *Tectonics*, *33*(2), 67–83. https://doi.org/10.1002/2012tc003224

Andreani, L., Gattacceca, J., Rangin, C., Martínez-Reyes, J., & Demory, F. (2014). Counterclockwise rotations in the Late Eocene–Oligocene volcanic fields of San Luis Potosí and Sierra de Guanajuato (eastern Mesa Central, Mexico). *Tectonophysics*, *637*, 289–304. https://doi.org/10.1016/j.tecto.2014.10.015

Arason, P., & Levi, S. (2010). Maximum likelihood solution for inclination-only data in paleomagnetism. *Geophysical Journal International*, *182*(2), 753–771. https://doi.org/10.1111/j.1365-246x.2010.04671.x

Arason, P., & Levi, S. (1990). Models of inclination shallowing during sediment compaction. *Journal of Geophysical Research*, *95*(B4), 4481–4499. https://doi.org/10.1029/jb095ib04p04481

Arriagada, C., Roperch, P., & Mpodozis, C. (2000). Clockwise block rotations along the eastern border of the Cordillera de Domeyko, northern Chile (22450– 23300S). *Tectonophysics*, *326*, 153–171. https://doi.org/10.1016/S0040-1951(00)00151-7

Arriagada, C., Roperch, P., Mpodozis, C., & Cobbold, P. R. (2008). Paleogene building of the Bolivian Orocline: Tectonic restoration of the central Andes in 2-D map view. *Tectonics*, *27*(6), TC6014. https://doi.org/10.1029/2008tc002269

Arriagada, C., Roperch, P., Mpodozis, C., Dupont- Nivet, G., Cobbold, P. R., Chauvin, A., & Cortés, J. (2003). Paleogene clockwise tectonic rotations in the forearc of central Andes, Antofagasta region, northern Chile. *Journal of Geophysical Research*, *108*(B1), 2032. https://doi.org/10.1029/2001JB001598

Aspden, J. A., Harrison, S. H., & Rundle, C. C. (1992). New geochronological control for the tectono-magmatic evolution of the metamorphic basement, Cordillera Real and El Oro Province of Ecuador. *Journal of South American Earth Sciences*, *6*(1–2), 77–96. https://doi.org/10.1016/0895-9811(92)90019-u

Aspden, J. A., & Litherland, M. (1992). The geology and Mesozoic collisional history of the Cordillera Real, Ecuador. *Tectonophysics*, *205*(1–3), 187–204. https://doi.org/10.1016/0040-1951(92)90426-7

Baby, P., Rivadeneira, M., Barragán, R., & Christophoul, F. (2013). Thick-skinned tectonics in the Oriente foreland basin of Ecuador. *Geological Society, London, Special Publications*, *377*(1), 59–76. https://doi.org/10.1144/sp377.1

Baize, S., Audin, L., Alvarado, A., Jomard, H., Bablon, M., Champenois, J., et al. (2020). Active Tectonics and Earthquake Geology Along the Pallatanga Fault, Central Andes of Ecuador. *Frontiers of Earth Science*, *8*, 193. https://doi.org/10.3389/feart.2020.00193

Barke, R., Lamb, S., & MacNiocaill, C. (2007). Late Cenozoic bending of the Bolivian Andes: New paleomagnetic and kinematic constraints. *Journal of Geophysical Research*, *112*(B1), B01101. https://doi.org/10.1029/2006jb004372

Bayona, G., Cortés, M., Jaramillo, C., Ojeda, G., Aristizabal, J. J., & Reyes-Harker, A. (2008). An integrated analysis of an orogen–sedimentary basin pair: Latest Cretaceous–Cenozoic evolution of the linked Eastern Cordillera orogen and the Llanos foreland basin of Colombia. *Geological Society of America Bulletin*, *120*(9–10), 1171–1197. https://doi.org/10.1130/b26187.1

Bayona, G., Rapalini, A., & Costanzo-Alvarez, V. (2006). Paleomagnetism in Mesozoic rocks of the northern Andes and its implications in Mesozoic tectonics of northwestern South America. *Earth Planets and Space*, *58*(10), 1255–1272. https://doi.org/10.1186/bf03352621

Beauval, C., Yepes, H., Bakun, W. H., Egred, J., Alvarado, A., & Singaucho, J. C. (2010). Locations and magnitudes of historical earthquakes in the Sierra of Ecuador (1587–1996). *Geophysical Journal International*, *181*(3), 1613–1633.

Beck, M. E., Jr, Burmester, R. R., Drake, R. E., & Riley, P. D. (1994). A tale of two continents: Some tectonic contrasts between the central Andes and the North American Cordillera, as illustrated by their paleomagnetic signatures. *Tectonics*, *13*(1), 215–224. https://doi.org/10.1029/93tc02398

Benitez, S. (1995). *Évolution géodynamique de la province côtière sud-équatorienne au Crétacé supérieur-Tertiaire, Université Joseph- Fourier - Grenoble I*.

Bleil, U., & Petersen, N. (1982). Magnetic properties of natural minerals. Numerical data and functional relationships in science and technology. *Group V: Geophysics and Space Research*, *1*, 308–365.

Branney, M. J., Kokelaar, B. P., & McConnell, B. J. (1992). The Bad Step Tuff: A lava-like rheomorphic ignimbrite in a calc-alkaline piecemeal caldera, English Lake District. *Bulletin of Volcanology*, *54*(3), 187–199. https://doi.org/10.1007/bf00278388

Bristow, C. R., & Parodiz, J. J. (1982). The stratigraphical paleontology of the tertiary non-maritime sediments of Ecuador. *Carnegie, Museum of Natural History Bulletin*, *19*, 53.

Butler, R. F., Richards, D. R., Sempere, T., & Marshall, L. G. (1995). Paleomagnetic determinations of vertical-axis tectonic rotations from Late Cretaceous and Paleocene strata of Bolivia. *Geology*, *23*(9), 799–802. https://doi.org/10.1130/0091-7613(1995)023<0799:PDOVAT>2.3.CO;2

Capitanio, F. A., Faccenna, C., Zlotnik, S., & Stegman, D. R. (2011). Subduction dynamics and the origin of Andean orogeny and the Bolivian orocline. *Nature*, *480*(7375), 83–86. https://doi.org/10.1038/nature10596

Cas, R. A. F., & Wright, J. V. (1987). *Volcanic Successions-Modern and Ancient. A Geological Approach to Processes, Products and Successions: London* (529). ALLEN and Unwin. https://doi.org/10.1007/978-94-009-3167-1

Casquet, C., Rapela, C. W., Pankhurst, R. J., Baldo, E. G., Galindo, C., Fanning, C. M., & Dahlquist, J. (2012). A history of Proterozoic terranes in southern South America: From Rodinia to Gondwana. *Geoscience Frontiers*, *3*(2), 137–145. https://doi.org/10.1016/j.gsf.2011.11.004

Cediel, F., Shaw, R. P., & Cáceres, C. (2003). Tectonic assembly of the northern Andean block. In C. Bartolini, R. T. Buffler, & J. Blickwede (Eds.), *The Circum-gulf of Mexico and the Caribbean: Hydrocarbon habitats, basin formation, and plate tectonics: AAPG Memoir 79* (pp. 815–848). https://doi.org/10.1306/m79877c37

Channell, J. E. T., Oldow, J. S., Catalano, R., & d'Argenio, B. (1990). Paleomagnetically determined rotations in the western Sicilian fold and thrust belt. *Tectonics*, *9*(4), 641–660. https://doi.org/10.1029/tc009i004p00641

Chiaradia, M., Fontboté, L., & Beate, B. (2004). Cenozoic continental arc magmatism and associated mineralization in Ecuador. *Mineralium Deposita*, *39*(2), 204–222. https://doi.org/10.1007/s00126-003-0397-5

Cifelli, F., & Mattei, M. (2010). Curved orogenic systems in the Italian Peninsula: A paleomagnetic. *Journal of the Virtual Explorer*, *36*. https://doi.org/10.3809/jvirtex.2010.00239

Daly, M. C. (1989). Correlations between Nazca/Farallon plate kinematics and forearc basin evolution in Ecuador. *Tectonics*, *8*(4), 769–790. https://doi.org/10.1029/tc008i004p00769

Davis, G. H., Reynolds, S. J., & Kluth, C. F. (1996). *Structural geology of rocks and regions*. John Wiley & Sons.

Deenen, M. H., Langereis, C. G., van Hinsbergen, D. J., & Biggin, A. J. (2011). Geomagnetic secular variation and the statistics of paleomagnetic directions. *Geophysical Journal International*, *186*(2), 509–520. https://doi.org/10.1111/j.1365-246x.2011.05050.x

Demarest, H. H., Jr (1983). Error analysis for the determination of tectonic rotation from paleomagnetic data. *Journal of Geophysical Research*, *88*(B5), 4321–4328. https://doi.org/10.1029/jb088ib05p04321

DeMets, C., Gordon, R. G., & Argus, D. F. (2010). Geologically current plate motions. *Geophysical Journal International*, *181*(1), 1–80. https://doi.org/10.1111/j.1365-246x.2009.04491.x

Dimate, C., Rivera, L., Taboada, A., Delouis, B., Osorio, A., Jimenez, E., & Gómez, I. (2003). The 19 January 1995 Tauramena (Colombia) earthquake: Geometry and stress regime. *Tectonophysics*, *363*(3–4), 159–180. https://doi.org/10.1016/s0040-1951(02)00670-4

Egbue, O., & Kellogg, J. (2010). Pleistocene to present North Andean "escape". *Tectonophysics*, *489*(1–4), 248–257. https://doi.org/10.1016/j.tecto.2010.04.021

Eguez, A., Alvarado, A., Yepes, H., Machette, M. N., Costa, C., Dart, R. L., & Bradley, L. A. (2003). Database and map of Quaternary faults and folds of Ecuador and its offshore regions. *US Geological Survey Open-File Report*, *3*, 289. https://doi.org/10.3133/ofr03289

Ekren, E. B., McIntyre, D. H., & Bennett, E. H. (1984). *High-temperature, large-volume, lavalike ash-flow tuffs without calderas in southwestern Idaho (No. 1272)*. USGPO.

England, P., Houseman, G., & Sonder, L. (1985). Length scales for continental deformation in convergent, divergent, and strike-slip environments: Analytical and approximate solutions for a thin viscous sheet model. *Journal of Geophysical Research*, *90*(B5), 3551–3557. https://doi.org/10.1029/jb090ib05p03551

England, P., & McKenzie, D. (1982). A thin viscous sheet model for continental deformation. *Geophysical Journal International*, *70*(2), 295–321. https://doi.org/10.1111/j.1365-246x.1982.tb04969.x

England, P., & Wells, R. E. (1991). Neogene rotations and quasicontinuous deformation of the Pacific Northwest continental margin. *Geology*, *19*(10), 978–981. https://doi.org/10.1130/0091-7613(1991)019<0978:NRAQDO>2.3.CO;2

Feldmann, R. M., Chirino-Galvez, L., Mason, G. L., Anderson, J. L., Duncan, P. W, Ward, R. A., & Salem, D. R., (1993). Fossil Penaeidae (Crustacea: Decapoda) from the Loyola Formation, Ecuador. *Annals of Carnegie Museum*, *62*, 229–243.

Fisher, R. A. (1953). Dispersion on a sphere. *Proceedings of the Royal Society of London - Series A: Mathematical and Physical Sciences*, *217*(1130), 295–305. https://doi.org/10.1098/rspa.1953.0064

Friedman, I., Long, W., & Smith, R. L. (1963). Viscosity and water content of rhyolite glass. *Journal of Geophysical Research*, *68*(24), 6523–6535. https://doi.org/10.1029/jz068i024p06523

Gansser, A. (1973). Facts and theories on the Andes. *Journal of the Geological Society, London*, *129*, 93–131. https://doi.org/10.1144/gsjgs.129.2.0093

Gattacceca, J., Deino, A., Rizzo, R., Jones, D. S., Henry, B., Beaudoin, B., & Vadeboin, F. (2007). Miocene rotation of Sardinia: New paleomagnetic and geochronological constraints and geodynamic implications. *Earth and Planetary Science Letters*, *258*(3–4), 359–377. https://doi.org/10.1016/j.epsl.2007.02.003

Gilder, S., Rousse, S., Farber, D., McNulty, B., Sempere, T., Torres, V., & Palacios, O. (2003). Post-Middle Oligocene origin of paleomagnetic rotations in Upper Permian to Lower Jurassic rocks from northern and southern Peru. *Earth and Planetary Science Letters*, *210*(1–2), 233–248. https://doi.org/10.1016/s0012-821x(03)00102-x

Global Volcanism Program (2013). *Volcanoes of the World, v. 4.9.0 (04 Jun 2020)*. In E. Venzke (Ed.). Smithsonian Institution. (Downloaded 09 Aug 2020). https://doi.org/10.5479/si.GVP.VOTW4-2013

Goossens, P. J., & Rose, W. I. (1973). Chemical composition and age determination of tholeitic rocks in the basic Cretaceous Complex, Ecuador. *Geological Society of America Bulletin*, *84*, 1043–1052. https://doi.org/10.1130/0016-7606(1973)84<1043:CCAADO>2.0.CO;2

Hernandez-Moreno, C., Speranza, F., & Di Chiara, A. (2014). Understanding kinematics of intra-arc transcurrent deformation: Paleomagnetic evidence from the Liquiñe-Ofqui fault zone (Chile, 38–41° S). *Tectonics*, *33*(10), 1964–1988.

Hernandez-Moreno, C., Speranza, F., & Di Chiara, A. (2016). Paleomagnetic rotation pattern of the southern Chile fore-arc sliver (38°S–42°S): A new tool to evaluate plate locking along subduction zones. *Journal of Geophysical Research: Solid Earth*, *121*(2), 469–490. 10.1002/2015JB012382

Hincapié-Gómez, S., Cardona, A., Jiménez, G., Monsalve, G., Ramírez-Hoyos, L., & Bayona, G. (2018). Paleomagnetic and gravimetrical reconnaissance of Cretaceous volcanic rocks from the Western Colombian Andes: Paleogeographic connections with the Caribbean Plate. *Studia Geophysica et Geodaetica*, *62*(3), 485–511. https://doi.org/10.1007/s11200-016-0678-y

Hungerbühler, D., Steinmann, M., Winkler, W., Seward, D., Egüez, A., Heller, F., & Ford, M. (1995). An integrated study of fill and deformation in the Andean intermontane basin of Nabón (Late Miocene), southern Ecuador. *Sedimentary Geology*, *96*(3–4), 257–279. https://doi.org/10.1016/0037-0738(94)00137-j

Hungerbühler, D., Steinmann, M., Winkler, W., Seward, D., Egüez, A., Peterson, D. E., & Hammer, C. (2002). Neogene stratigraphy and Andean geodynamics of southern Ecuador. *Earth-Science Reviews*, *57*(1–2), 75–124. https://doi.org/10.1016/s0012-8252(01)00071-x

Iaffaldano, G., & Bunge, H. P. (2008). Strong plate coupling along the Nazca–South America convergent margin. *Geology*, *36*(6), 443–446. https://doi.org/10.1130/g24489a.1

Isacks, B. L. (1988). Uplift of the central Andean plateau and bending of the Bolivian orocline. *Journal of Geophysical Research*, *93*(B4), 3211–3231. https://doi.org/10.1029/jb093ib04p03211

Jaillard, E., Laubacher, G., Bengtson, P., Dhondt, A. V., & Bulot, L. G. (1999). Stratigraphy and evolution of the Cretaceous forearc Celica- Lancones basin of southwestern Ecuador. *Journal of South American Earth Sciences*, *12*(1), 51–68. https://doi.org/10.1016/S0895-9811(99)00006-1

Jaillard, É., Ordoñez, M., Benitez, S., Berrones, G., Jiménez, N., Montenegro, G., & Zambrano, I. (1995). Basin development in an accretionary, oceanic-floored fore-arc setting: Southern coastal Ecuador during late Cretaceous-late Eocene time. In A. J. Tankard, S. R. Suarez, & H. J. Welsink (Eds.), *Petroleum basins of south America* (pp. 615–631). AAPG. https://doi.org/10.1306/m62593c32

Jaillard, E., Ordonez, M., Suárez, J., Toro, J., Iza, D., & Lugo, W. (2004). Stratigraphy of the late Cretaceous–Paleogene deposits of the cordillera occidental of central Ecuador: Geodynamic implications. *Journal of South American Earth Sciences*, *17*(1), 49–58. https://doi.org/10.1016/j.jsames.2004.05.003

Jiménez, G., Speranza, F., Faccenna, C., Bayona, G., & Mora, A. (2014). Paleomagnetism and magnetic fabric of the Eastern Cordillera of Colombia: Evidence for oblique convergence and non-rotational reactivation of a Mesozoic intracontinental rift. *Tectonics*, *33*(11), 2233–2260. https://doi.org/10.1002/2014tc003532

Kerr, A. C., Aspden, J. A., Tarney, J., & Pilatasig, L. F. (2002). The nature and provenance of accreted oceanic terranes in western Ecuador: Geochemical and tectonic constraints. *Journal of the Geological Society*, *159*(5), 577–594. https://doi.org/10.1144/0016-764901-151

Kerr, A. C., Marriner, G. F., Tarney, J., Nivia, A., Saunders, A. D., Thirlwall, M. F., & Sinton, C. W. (1997). Cretaceous basaltic terranes in western Colombia: Elemental, chronological and Sr-Nd isotopic constraints on petrogenesis. *Journal of Petrology*, *38*(6), 677–702. https://doi.org/10.1093/petroj/38.6.677

Kerr, A. C., & Tarney, J. (2005). Tectonic evolution of the Caribbean and northwestern South America: The case for accretion of two Late Cretaceous oceanic plateaus. *Geology*, *33*(4), 269–272. https://doi.org/10.1130/g21109.1

Kirschvink, J. L. (1980). The least-squares line and plane and the analysis of paleomagnetic data. *Geophysical Journal International*, *62*(3), 699–718. https://doi.org/10.1111/j.1365-246x.1980.tb02601.x

Lamb, S. (2001a). Vertical axis rotation in the Bolivian orocline, South America: 1. Paleomagnetic analysis of Cretaceous and Cenozoic rocks. *Journal of Geophysical Research*, *106*, 26605–26632. https://doi.org/10.1029/10.1029/2001jb900012

Lamb, S. (2001b). Vertical axis rotation in the Bolivian orocline, South America: 2. Kinematic and dynamical implications. *Journal of Geophysical Research*, *106*, 26633–26653. https://doi.org/10.1029/2001JB000203

Lamb, S., & Davis, P. (2003). Cenozoic climate change as a possible cause for the rise of the Andes. *Nature*, *425*(6960), 792–797. https://doi.org/10.1038/nature02049

Lamb, S. H. (1987). A model for tectonic rotations about a vertical axis. *Earth and Planetary Science Letters*, *84*(1), 75–86. https://doi.org/10.1016/0012-821X(87)90178-6

Lapierre, H., Bosch, D., Dupuis, V., Polvé, M., Maury, R. C., Hernandez, J., et al. (2000). Multiple plume events in the genesis of the peri-Caribbean Cretaceous oceanic plateau province. *Journal of Geophysical Research*, *105*(B4), 8403–8421. https://doi.org/10.1029/1998jb900091

Lavenu, A., Winter, T., & Dávila, F. (1995). A Pliocene–Quaternary compressional basin in the Interandean depression, central Ecuador. *Geophysical Journal International*, *121*(1), 279–300. https://doi.org/10.1111/j.1365-246x.1995.tb03527.x

Lebras, M., Megard, F., Dupuy, C., & Dostal, J. (1987). Geochemistry and tectonic setting of pre-collision Cretaceous and Paleogene volcanic rocks of Ecuador. *Geological Society of America Bulletin*, *99*(4), 569–578. https://doi.org/10.1130/0016-7606(1987)99<569:GATSOP>2.0.CO;2

Legrand, D., Baby, P., Bondoux, F., Dorbath, C., De Berc, S. B., & Rivadeneira, M. (2005). The 1999–2000 seismic experiment of Macas swarm (Ecuador) in relation with rift inversion in Subandean foothills. *Tectonophysics*, *395*(1–2), 67–80. https://doi.org/10.1016/j.tecto.2004.09.008

Litherland, M., Aspden, J. A., & Jemielita, R. A. (1994). *The metamorphic belts of ecuador*. (pp. 147). Overseas Mem. Br. Geol. Surv.

Luzieux, L. D. A., Heller, F., Spikings, R., Vallejo, C. F., & Winkler, W. (2006). Origin and Cretaceous tectonic history of the coastal Ecuadorian forearc between 1 N and 3 S: Paleomagnetic, radiometric and fossil evidence. *Earth and Planetary Science Letters*, *249*(3–4), 400–414. https://doi.org/10.1016/j.epsl.2006.07.008

MacDonald, W. D., & Opdyke, N. D. (1972). Tectonic rotations suggested by paleomagnetic results from northern Colombia, South America. *Journal of Geophysical Research*, *77*(29), 5720–5730. https://doi.org/10.1029/jb077i029p05720

Macedo, J., & Marshak, S. (1999). Controls on the geometry of fold-thrust belt salients. *Geological Society of America Bulletin*, *111*(12), 1808–1822. https://doi.org/10.1130/0016-7606(1999)111<1808:COTGOF>2.3.CO;2

MacFadden, B. J., Anaya, F., & Swisher, C. C., III (1995). Neogene paleomagnetism and oroclinal bending of the central Andes of Bolivia. *Journal of Geophysical Research*, *100*(B5), 8153–8167. https://doi.org/10.1029/95jb00149

Maffione, M., Speranza, F., & Faccenna, C. (2009). Bending of the Bolivian orocline and growth of the central Andean plateau: Paleomagnetic and structural constraints from the Eastern Cordillera (22–24 S, NW Argentina). *Tectonics*, *28*(4), TC4006. https://doi.org/10.1029/2008tc002402

Martínez-García, B., Corrochano, D., Suárez-Hernando, O., Solís-Alulima, B., Suárez-Bilbao, A., Ordiales, A., & Murelaga, X. (2017). Benthic Foraminifera and Ostracoda from Middle-Upper Miocene Sequences of Southern Ecuador. *Ameghiniana*, *54*(2), 177–207. https://doi.org/10.5710/amgh.18.10.2016.2938

Márton, E., Trajanova, M., Zupančič, N., & Jelen, B. (2006). Formation, uplift and tectonic integration of a Periadriatic intrusive complex (Pohorje, Slovenia) as reflected in magnetic parameters and paleomagnetic directions. *Geophysical Journal International*, *167*(3), 1148–1159. https://doi.org/10.1111/j.1365-246x.2006.03098.x

Massonne, H. J., & Toulkeridis, T. (2012). Widespread relics of high-pressure metamorphism confirm major terrane accretion in Ecuador: A new example from the Northern Andes. *International Geology Review*, *54*(1), 67–80. https://doi.org/10.1080/00206814.2010.498907

McClelland, E., Wilson, C. J., & Bardot, L. (2004). Paleotemperature determinations for the 1.8-ka Taupo ignimbrite, New Zealand, and implications for the emplacement history of a high-velocity pyroclastic flow. *Bulletin of Volcanology*, *66*(6), 492–513. https://doi.org/10.1007/s00445-003-0335-5

McFadden, P. L. (1990). A new fold test for paleomagnetic studies. *Geophysical Journal International*, *103*(1), 163–169. https://doi.org/10.1111/j.1365-246x.1990.tb01761.x

McFadden, P. L., & McElhinny, M. W. (1990). Classification of the reversal test in palaeomagnetism. *Geophysical Journal International*, *103*(3), 725–729. https://doi.org/10.1111/j.1365-246x.1990.tb05683.x

McKenzie, D., & Jackson, J. (1986). A block model of distributed deformation by faulting. *Journal of the Geological Society*, *143*(2), 349–353. https://doi.org/10.1144/gsjgs.143.2.0349

McQuarrie, N. (2002). Initial plate geometry, shortening variations, and evolution of the Bolivian orocline. *Geology*, *30*(10), 867–870. https://doi.org/10.1130/0091-7613(2002)030<0867:ipgsva>2.0.co;2

Merrill, R. T., McElhinny, M. W., & McFadden, P. L. (1996). *The magnetic field of the Earth: Paleomagnetism, the core, and the deep mantle*. Elsevier.

Montes, C., Bayona, G., Cardona, A., Buchs, D. M., Silva, C. A., Morón, S., et al. (2012). Arc-continent collision and orocline formation: Closing of the Central American seaway. *Journal of Geophysical Research*, *117*, B04105. https://doi.org/10.1029/2011jb008959

Montes, C., Hatcher, R. D., Jr, & Restrepo-Pace, P. A. (2005). Tectonic reconstruction of the northern Andean blocks: Oblique convergence and rotations derived from the kinematics of the Piedras–Girardot area, Colombia. *Tectonophysics*, *399*(1–4), 221–250. https://doi.org/10.1016/j.tecto.2004.12.024

Montgomery, D. R., Balco, G., & Willett, S. D. (2001). Climate, tectonics, and the morphology of the Andes. *Geology*, *29*(7), 579–582. https://doi.org/10.1130/0091-7613(2001)029<0579:CTATMO>2.0.CO;2

Mora, J. A., Oncken, O., Le Breton, E., Ibánez-Mejia, M., Faccenna, C., Veloza, G., et al. (2017). Linking Late Cretaceous to Eocene tectonostratigraphy of the San Jacinto fold belt of NW Colombia with Caribbean Plateau collision and flat subduction. *Tectonics*, *36*(11), 2599–2629. https://doi.org/10.1002/2017tc004612

Mulas, M., Aviles Moran, H. S., Flor Jimenez, M. A., Sanclemente Ordoñez, E. R., Le Pennec, J. L., & Larreta Torres, E. W. (2017). *The Pucará Caldera: Evidences for a miocene caldera-forming eruption*. AGU. FM, 2017, V23E–0528.

Müller, J. P., Kley, J., & Jacobshagen, V. (2002). Structure and Cenozoic kinematics of the Eastern Cordillera, southern Bolivia (21°S). *Tectonics*, *21*(5), 1037. https://doi.org/10.1029/2001TC001340

Narea, K., Peña, M., Bascuñán, S., Becerra, J., Gómez, I., Deckart, K., et al. (2015). Paleomagnetism of Permo-Triassic and Cretaceous rocks from the Antofagasta region, northern Chile. *Journal of South American Earth Sciences*, *64*, 261–272. https://doi.org/10.1016/j.jsames.2015.09.008

Nelson, M., & Jones, C. (1987). Paleomagnetism and crustal rotations along a shear zone, Las Vegas Range, southern Nevada. *Tectonics*, *6*(1), 13–33. https://doi.org/10.1029/TC006i001p00013

Noblet, C., & Marocco, R. (1989). Lacustrine metaturbidites in an intermontane strike-slip basin: The Miocene Cuenca Basin of South Ecuador. In *Paper present in the International Symposium on Intermontane Basins: Geology and Resources* (pp. 282–293).

Nocquet, J. M., Villegas-Lanza, J. C., Chlieh, M., Mothes, P. A., Rolandone, F., Jarrin, P., et al. (2014). Motion of continental slivers and creeping subduction in the northern Andes. *Nature Geoscience*, *7*(4), 287–291. https://doi.org/10.1038/ngeo2099

Nuttall, C. P. (1990). A review of the tertiary non-marine molluscan faunas of the Pebasian and other inland basins of north-western South America. *Bulletin of the British Museum, Natural History. Geology*, *45*(2).

Oldow, J. S., Channell, J. E. T., Catalano, R., & D'Argenio, B. (1990). Contemporaneous thrusting and large-scale rotations in the western Sicilian fold and thrust belt. *Tectonics*, *9*(4), 661–681. https://doi.org/10.1029/TC009i004p00661

Pardo-Casas, F., & Molnar, P. (1987). Relative motion of the Nazca (Farallon) and South American plates since Late Cretaceous time. *Tectonics*, *6*(3), 233–248. https://doi.org/10.1016/0198-0254(87)96011-0

Paris, G. (2000). *Map and database of Quaternary faults and folds in Colombia and its offshore regions*. (pp. 1–61). US Geological Survey. https://doi.org/10.3133/ofr00284

Pellegrino, A. G., Zhang, B., Speranza, F., Maniscalco, R., Yin, C., Hernandez-Moreno, C., & Winkler, A. (2018). Tectonics and paleomagnetic rotation pattern of Yunnan (24 N–25 N, China): Gaoligong fault shear versus megablock drift. *Tectonics*, *37*(5), 1524–1551. https://doi.org/10.1029/2017tc004899

Pennington, W. D. (1981). Subduction of the eastern Panama Basin and seismotectonics of northwestern South America. *Journal of Geophysical Research*, *86*(B11), 10753–10770. https://doi.org/10.1029/jb086ib11p10753

Pérez, O. J., Wesnousky, S. G., De La Rosa, R., Márquez, J., Uzcátegui, R., Quintero, C., et al. (2018). On the interaction of the North Andes plate with the Caribbean and South American plates in northwestern South America from GPS geodesy and seismic data. *Geophysical Journal International*, *214*(3), 1986–2001. https://doi.org/10.1093/gji/ggy230

Piper, J. D. A., Tatar, O., & Gürsoy, H. (1997). Deformational behavior of continental lithosphere deduced from block rotations across the North Anatolian fault zone in Turkey. *Earth and Planetary Science Letters*, *150*(3–4), 191–203. https://doi.org/10.1016/s0012-821x(97)00103-9

Pousse-Beltran, L., Vassallo, R., Audemard, F., Jouanne, F., Carcaillet, J., Pathier, E., & Volat, M. (2017). Pleistocene slip rates on the Boconó fault along the North Andean Block plate boundary, Venezuela. *Tectonics*, *36*(7), 1207–1231.

Pratt, W. T., Duque, P., & Ponce, M. (2005). An autochthonous geological model for the eastern Andes of Ecuador. *Tectonophysics*, *399*(1–4), 251–278. https://doi.org/10.1016/j.tecto.2004.12.025

Prezzi, C., Caffe, P. J., & Somoza, R. (2004). New paleomagnetic data from the northern Puna and western Cordillera Oriental, Argentina: A new insight on the timing of rotational deformation. *Journal of Geodynamics*, *38*(2), 93–115. https://doi.org/10.1016/j.jog.2004.05.001

Prezzi, C., & Vilas, J. (1998). New evidence of clockwise vertical axis rotations south of the Arica elbow (Argentine Puna). *Tectonophysics*, *292*, 85–100. https://doi.org/10.1016/S0040-1951(98)00058-4

Prezzi, C. B., & Alonso, R. N. (2002). New paleomagnetic data from the northern Argentine Puna: Central Andes rotation pattern reanalyzed. *Journal of Geophysical Research*, *107*(B2), EPM-1. https://doi.org/10.1029/2001jb000225

Puigdomenech, C., Somoza, R., Tomlinson, A., & Renda, E. M. (2020). Paleomagnetic data from the Precordillera of northern Chile: A multiphase rotation history related to a multiphase deformational history. *Tectonophysics*, *791*, 228569. https://doi.org/10.1016/j.tecto.2020.228569

Quane, S. L., Russell, J. K., & Friedlander, E. A. (2009). Time scales of compaction in volcanic systems. *Geology*, *37*(5), 471–474. https://doi.org/10.1130/g25625a.1

Ramos, V. A. (2009). Anatomy and global context of the Andes: Main geologic features and the Andean orogenic cycle. *Backbone of the Americas: shallow subduction, Plateau Uplift, and Ridge and Terrane collision*, *204*, 31–65. https://doi.org/10.1130/2009.1204(02)

Randall, D. E., Taylor, G. K., & Grocott, J. (1996). Major crustal rotations in the Andean margin: Paleomagnetic results from the Coastal Cordillera of northern Chile. *Journal of Geophysical Research*, *101*(15), 15783–15798. https://doi.org/10.1029/96JB00817

Randall, K., Lamb, S., & Mac Niocaill, C. (2011). Large tectonic rotations in a wide zone of Neogene distributed dextral shear, northeastern South Island, New Zealand. *Tectonophysics*, *509*(3–4), 165–180. https://doi.org/10.1016/j.tecto.2011.05.006

Reynaud, C., Jaillard, É., Lapierre, H., Mamberti, M., & Mascle, G. H. (1999). Oceanic plateau and island arcs of southwestern Ecuador: Their place in the geodynamic evolution of northwestern South America. *Tectonophysics*, *307*(3–4), 235–254. https://doi.org/10.1016/s0040-1951(99)00099-2

Riehle, J. R. (1973). Calculated compaction profiles of rhyolitic ash-flow tuffs. *Geological Society of America Bulletin*, *84*(7), 2193–2216. https://doi.org/10.1130/0016-7606(1973)84<2193:CCPORA>2.0.CO;2

Riehle, J. R., Miller, T. F., & Bailey, R. A. (1995). Cooling, degassing and compaction of rhyolitic ash flow tuffs: A computational model. *Bulletin of Volcanology*, *57*(5), 319–336. https://doi.org/10.1007/s004450050097

Riller, U., & Oncken, O. (2003). Growth of the Central Andean Plateau by tectonic segmentation is controlled by the gradient in crustal shortening. *The Journal of Geology*, *111*(3), 367–384. https://doi.org/10.1086/373974

Roddaz, M., Hermoza, W., Mora, A., Baby, P., Parra, M., Christophoul, F., & Espurt, N. (2010). *Cenozoic sedimentary evolution of the Amazonian foreland basin system. Amazonia, landscape and species evolution: A look into the past* (pp. 61–88). Blackwell-Wiley.

Ron, H., Freund, R., Garfunkel, Z., & Nur, A. (1984). Block rotation by strike-slip faulting: Structural and paleomagnetic evidence. *Journal of Geophysical Research*, *89*(B7), 6256–6270. https://doi.org/10.1029/jb089ib07p06256

Roperch, P., & Carlier, G. (1992). Palcomagnetism of Mesozoic rocks from the central Andes of southern Peru: Importance of rotations in the development of the Bolivian orocline. *Journal of Geophysical Research*, *97*(17), 17233 – 17249. https://doi.org/10.1029/92JB01291

Roperch, P., Megard, F., Laj, C., Mourier, T., Clube, T. M., & Noblet, C. (1987). Rotated oceanic blocks in western Ecuador. *Geophysical Research Letters*, *14*(5), 558–561. https://doi.org/10.1029/gl014i005p00558

Rousse, S., Gilder, S., Farber, D., McNulty, B., Patriat, P., Torres, V., & Sempere, T. (2003). Paleomagnetic tracking of mountain building in the Peruvian Andes since 10 Ma. *Tectonics*, *22*(5), 1048. https://doi.org/10.1029/2003tc001508

Rousse, S., Gilder, S., Fornari, M., & Sempere, T. (2005). Insight into the Neogene tectonic history of the northern Bolivian Orocline from new paleomagnetic and geochronologic data. *Tectonics*, *24*(6), TC6007. https://doi.org/10.1029/2004tc001760

Russo, R. M., & Silver, P. G. (1996). Cordillera formation, mantle dynamics, and the Wilson cycle. *Geology*, *24*(6), 511–514. https://doi.org/10.1130/0091-7613(1996)024<0511:CFMDAT>2.3.CO;2

Shaanan, U., Rosenbaum, G., Pisarevsky, S., & Speranza, F. (2015). Paleomagnetic data from the New England Orogen (eastern Australia) and implications for oroclinal bending. *Tectonophysics*, *664*, 182–190. https://doi.org/10.1016/j.tecto.2015.09.018

Siravo, G. (2021). *PhD [data set]. Tectonics*. Zenodo. https://doi.org/10.5281/zenodo.5040097

Siravo, G., Speranza, F., Hernandez-Moreno, C., & Di Chiara, A. (2020). Orogen-parallel transition from a decoupled fore-arc Sliver to Andean-Type mountain chain: Paleomagnetic and geologic evidence from Southern Chile (37–39° S). *Tectonics*, *39*(2), e2019TC005881. https://doi.org/10.1029/2019tc005881

Sobolev, S. V., & Babeyko, A. Y. (2005). What drives orogeny in the Andes? *Geology*, *33*(8), 617–620. https://doi.org/10.1130/g21557.1

Somoza, R., Singer, S., & Coira, B. (1996). Paleomagnetism of upper Miocene ignimbrites at the Puna: An analysis of vertical-axis rotations in the central Andes. *Journal of Geophysical Research*, *101*, 11387–11400. https://doi.org/10.1029/95JB03467

Sonder, L. J., & England, P. (1986). Vertical averages of rheology of the continental lithosphere: Relation to thin sheet parameters. *Earth and Planetary Science Letters*, *77*(1), 81–90. https://doi.org/10.1016/0012-821x(86)90134-2

Sonder, L. J., England, P. C., & Houseman, G. A. (1986). Continuum calculations of continental deformation in transcurrent environments. *Journal of Geophysical Research*, *91*(B5), 4797–4810. https://doi.org/10.1029/jb091ib05p04797

Sonder, L. J., Jones, C. H., Salyards, S. L., & Murphy, K. M. (1994). Vertical axis rotations in the Las Vegas Valley Shear Zone, southern Nevada: Paleomagnetic constraints on kinematics and dynamics of block rotations. *Tectonics*, *13*(4), 769–788. https://doi.org/10.1029/94tc00352

Speranza, F., Hernandez-Moreno, C., Avellone, G., Gasparo Morticelli, M., Agate, M., Sulli, A., & Di Stefano, E. (2018). Understanding paleomagnetic rotations in Sicily: Thrust versus strike-slip tectonics. *Tectonics*, *37*(4), 1138–1158. https://doi.org/10.1002/2017tc004815

Spikings, R. A., Crowhurst, P. V., Winkler, W., & Villagomez, D. (2010). Syn-and post-accretionary cooling history of the Ecuadorian Andes constrained by their in-situ and detrital thermochronometric record. *Journal of South American Earth Sciences*, *30*(3–4), 121–133. https://doi.org/10.1016/j.jsames.2010.04.002

Spikings, R. A., Winkler, W., Hughes, R. A., & Handler, R. (2005). Thermochronology of allochthonous terranes in Ecuador: Unraveling the accretionary and post-accretionary history of the Northern Andes. *Tectonophysics*, *399*(1–4), 195–220. https://doi.org/10.1016/j.tecto.2004.12.023

Spikings, R. A., Winkler, W., Seward, D., & Handler, R. (2001). Along-strike variations in the thermal and tectonic response of the continental Ecuadorian Andes to the collision with heterogeneous oceanic crust. *Earth and Planetary Science Letters*, *186*(1), 57–73. https://doi.org/10.1016/s0012-821x(01)00225-4

Steinmann, M. (1997). *The Cuenca basin of southern Ecuador: Tectono-sedimentary history and the Tertiary andean evolution (Doctoral dissertation)*. ETH Zurich.

Steinmann, M., Hungerbühler, D., Seward, D., & Winkler, W. (1999). Neogene tectonic evolution and exhumation of the southern Ecuadorian Andes: A combined stratigraphy and fission-track approach. *Tectonophysics*, *307*(3–4), 255–276. https://doi.org/10.1016/s0040-1951(99)00100-6

Strecker, M. R., Cerveny, P., Bloom, A. L., & Malizia, D. (1989). Late Cenozoic tectonism and landscape development in the foreland of the Andes: Northern Sierras Pampeanas (26–28 S), Argentina. *Tectonics*, *8*(3), 517–534. https://doi.org/10.1029/tc008i003p00517

Tibaldi, A., & Ferrari, L. (1992). Latest Pleistocene-Holocene tectonics of the Ecuadorian Andes. *Tectonophysics*, *205*(1–3), 109–125. https://doi.org/10.1016/0040-1951(92)90421-2

Todrani, A., Zhang, B., Speranza, F., & Chen, S. (2020). Paleomagnetism of the middle Cenozoic Mula Basin (East Tibet): Evidence for km-scale crustal blocks rotated by midlower crust drag. *Geochemistry, Geophysics, Geosystems*, *21*(9), e2020GC009225. https://doi.org/10.1029/2020gc009225

Torsvik, T. H., Van der Voo, R., Preeden, U., Mac Niocaill, C., Steinberger, B., Doubrovine, P. V., & Meert, J. G. (2012). Phanerozoic polar wander, paleogeography and dynamics. *Earth-Science Reviews*, *114*(3–4), 325–368. https://doi.org/10.1016/j.earscirev.2012.06.007

Trenkamp, R., Kellogg, J. N., Freymueller, J. T., & Mora, H. P. (2002). Wide plate margin deformation, southern Central America and northwestern South America, CASA GPS observations. *Journal of South American Earth Sciences*, *15*(2), 157–171. https://doi.org/10.1016/s0895-9811(02)00018-4

Vallejo, C., Spikings, R. A., Horton, B. K., Luzieux, L., Romero, C., Winkler, W., & Thomsen, T. B. (2019). Late Cretaceous to Miocene stratigraphy and provenance of the coastal forearc and Western Cordillera of Ecuador: Evidence for accretion of a single oceanic plateau fragment. In *Andean tectonics* (pp. 209–236). Elsevier. https://doi.org/10.1016/b978-0-12-816009-1.00010-1

Vallejo, C., Winkler, W., Spikings, R. A., Luzieux, L., Heller, F., & Bussy, F. (2009). Mode and timing of terrane accretion in the forearc of the Andes in Ecuador. Back of the Americas: Shallow, subduction, plateau uplift, and ridge and terrane collision. *Memoirs (Geological Society of America)*, *204*, 197. https://doi.org/10.1130/2009.1204(09)

Villagómez, D. (2003). *Evolución Plio-cuaternaria del Valle Interandino Central en Ecuador (zona Quito-Guayllabamba-San Antonio de Pichincha) (Doctoral dissertation, Tesis de grado*. EPN-Quito).

Villegas-Lanza, J. C., Chlieh, M., Cavalié, O., Tavera, H., Baby, P., Chire-Chira, J., & Nocquet, J. M. (2016). Active tectonics of Peru: Heterogeneous interseismic coupling along the Nazca megathrust, rigid motion of the Peruvian Sliver, and Subandean shortening accommodation. *Journal of Geophysical Research*, *121*(10), 7371–7394. 10.1002/2016JB013080

Wdowinski, S., O'Connell, R. J., & England, P. (1989). A continuum model of continental deformation above subduction zones: Application to the Andes and the Aegean. *Journal of Geophysical Research*, *94*(B8), 10331–10346. https://doi.org/10.1029/jb094ib08p10331

Weil, A. B., Yonkee, A., & Sussman, A. (2010). Reconstructing the kinematic evolution of curved mountain belts: A paleomagnetic study of Triassic red beds from the Wyoming salient, Sevier thrust belt. *U.S.A. Geological Society of America Bulletin*, *122*, 3–23. https://doi.org/10.1130/b26483.1

Winkler, W., Villagómez, D., Spikings, R., Abegglen, P., Egüez, A., & Egüez, A. (2005). The Chota basin and its significance for the inception and tectonic setting of the inter-Andean depression in Ecuador. *Journal of South American Earth Sciences*, *19*(1), 5–19. https://doi.org/10.1016/j.jsames.2004.06.006

Winter, T., Avouac, J. P., & Lavenu, A. (1993). Late Quaternary kinematics of the Pallatanga strike-slip fault (Central Ecuador) from topographic measurements of displaced morphological features. *Geophysical Journal International*, *115*(3), 905–920. https://doi.org/10.1111/j.1365-246x.1993.tb01500.x

Winter, T., & Lavenu, A. (1989). Morphological and microtectonic evidence for a major active right-lateral strike slip fault across central Ecuador. *Tectonophysics*, *399*(1), 331–350.

Witt, C., & Bourgois, J. (2010). Forearc basin formation in the tectonic wake of a collision-driven, coastwise migrating crustal block: The example of the North Andean block and the extensional Gulf of Guayaquil-Tumbes Basin (Ecuador-Peru border area). *GSA Bulletin*, *122*(1–2), 89–108. https://doi.org/10.1130/b26386.1

Witt, C., Bourgois, J., Michaud, F., Ordoñez, M., Jiménez, N., & Sosson, M. (2006). Development of the Gulf of Guayaquil (Ecuador) during the Quaternary as an effect of the North Andean block tectonic escape. *Tectonics*, *25*(3), TC3017. https://doi.org/10.1029/2004tc001723

Yagi, K. E. N. Z. O. (1966). Experimental study on pumice and obsidian. *Bulletin Volcanologique*, *29*(1), 559–572. https://doi.org/10.1007/bf02597176

Yáñez, G., & Cembrano, J. (2004). Role of viscous plate coupling in the late Tertiary Andean tectonics. *Journal of Geophysical Research*, *109*(B2), B02407. https://doi.org/10.1029/2003jb002494

Yuan, X., Sobolev, S. V., Kind, R., Oncken, O., Bock, G., Asch, G., et al. (2000). Subduction and collision processes in the Central Andes constrained by converted seismic phases. *Nature*, *408*(6815), 958–961. https://doi.org/10.1038/35050073

Zijderveld, J. D. (1967). A. C. Demagnetization of rocks: Analysis of results. In D. W. Collinson, K. M. Creer, & S. K. Runcorn (Eds.), *Methods in pleomagnetism* (pp. 254–286). New York. Elsevier.